

Faster Preparation of Multi-qubit Entanglement with Higher Success Rates

B.-B. Liu,^{1,*} Shi-Lei Su^{*,1,2,†} Y.-L. Zuo,^{3,4} Gang Chen,^{1,‡} Ş. K. Özdemir,⁵ and H. Jing^{3,§}

¹*School of Physics and Laboratory of Zhongyuan Light,
Zhengzhou University, Zhengzhou 450001, China*

²*Institute of Quantum Materials and Physics, Henan Academy of Sciences, Zhengzhou 450046, China**

³*Key Laboratory of Low-Dimensional Quantum Structures and Quantum Control of Ministry of Education,
Department of Physics and Synergetic Innovation Center for Quantum Effects and Applications,
Hunan Normal University, Changsha 410081, China*

⁴*School of Physics and Chemistry, Hunan First Normal University, Changsha 410205, China*

⁵*Department of Engineering Science and Mechanics, Pennsylvania State University,
University Park, State College, PA 16802, United States of America*

A noteworthy discovery in recent research is that the process of two-qubit quantum entanglement preparation can be significantly accelerated near the exceptional point (EP) or spectral coalescence of non-Hermitian systems, as compared to conventional Hermitian setups. Nevertheless, a significant obstacle for quantum EP-based devices is their limited success rate in generating highly entangled states, stemming from an inherent trade-off relation between entanglement degree and success rate in all lossy EP systems. Our study demonstrates that this limitation can be effectively overcome by harnessing a truly parity-time (\mathcal{PT})-symmetric system, which possesses balanced gain and loss, thereby enabling maximal entanglement with rapid speed, high success rates, and greater resilience to non-resonant errors. We believe this approach can efficiently prepare multi-qubit entanglement and use not only bipartite but also tripartite entanglement as examples to illustrate, even when the precise gain-loss balance is not strictly maintained. Our analytical findings are in excellent agreement with numerical simulations, confirming the potential of \mathcal{PT} -devices as a powerful tool for creating and engineering diverse quantum resources for applications in quantum information technology.

I. INTRODUCTION

Quantum entanglement, as the cornerstone of quantum information science and technology [1], plays a central role in large-scale quantum computing [2–5], secure quantum communications [6–10], and high-performance quantum metrology [11–14]. To avoid detrimental effects of noises on the typically fragile quantumness, it is highly desired to realize fast preparations of entanglement in practice [15–18], which is typically limited by the coupling strength of qubits in conventional Hermitian systems. An appealing strategy to overcome this limit is to utilize the exceptional points (EPs) or the spectral coalescence of non-Hermitian systems to speed up quantum evolution processes [19, 20] and the scheme of accelerating entanglement preparation have been proposed recently [21]. However, a major challenge for such quantum EP devices is the very low success rate in creating highly entangled states, due to a fundamental trade-off relation between the entanglement degree and the success rate in all lossy EP dynamics.

In contrast to complex energy spectrums exhibited by lossy EP systems, \mathcal{PT} -symmetric systems with balanced gain and loss, which remains invariant under the joint operator of parity and time reversal, possess entirely real spectrum similar with Hermitian systems [22–28],

hence preserving conserved dynamics [29–35] and featuring superior performances in sensing applications [36–40], optical engineering [41–45], and phonon-laser operations [46, 47], to name only a few [48–56]. We note that such active \mathcal{PT} -devices have been demonstrated in recent experiments [41, 42, 57–61], examples include optics and photonics [62–71], spin system [72], acoustics [73, 74], and various lattices [75–77].

In this manuscript, we show that the trade-off relation in all lossy dynamics is well beaten by using a truly \mathcal{PT} -symmetric system and find that \mathcal{PT} -symmetric systems allow much faster preparations of high-degree quantum entanglement. This ability, as far as we know, has not been reported in previous works and can be important for practical quantum techniques requiring high-quality entanglement.

II. BASIC THEORY AND METHOD

Non-Hermitian systems have demonstrated the potential to accelerate quantum evolution, thereby inspiring various accelerated entanglement preparation schemes. For the preparation of multi-qubit entanglement as depicted in Fig. 1(a), the Hamiltonian at the simplest level can be described by

$$H = \sum_{n=1}^N H_n + J \sum_{n \neq m=1}^N \sigma_n^+ \sigma_m^-, \quad (1)$$

in which the coupling strength between any two qubits is denoted by J , for the passive \mathcal{PT} -symmetric (all lossy) scenarios, where the loss executes in the upper energy

* These authors contributed equally to this work.

† slsu@zzu.edu.cn

‡ chengang971@163.com

§ jinghui73@foxmail.com

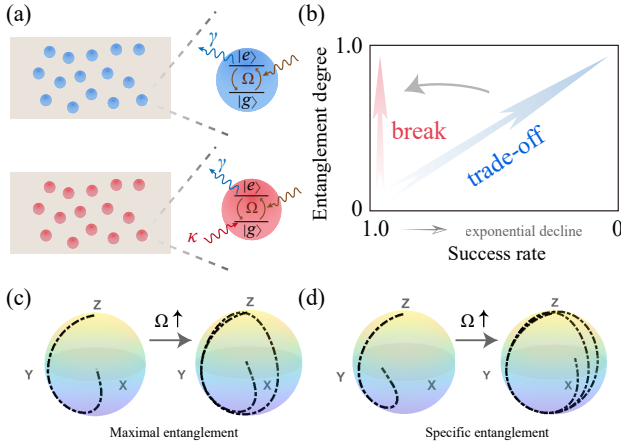


FIG. 1. (a) Schematic of multi-body all lossy EP (top) and truly \mathcal{PT} -symmetric (bottom) systems. Ω , γ and κ represent the driven amplitude, loss and gain, respectively. (b) A diagram of the trade-off relation between the entanglement degree and success rate for the all lossy EP system, and the truly \mathcal{PT} -symmetric system can break this relation. Schematic of dynamic trajectory of reduced single qubit on the Bloch sphere after selecting optimal parameters for the preparation of maximal (c) and specific (d) entanglement. For global entanglement, the trajectory lies within the Bloch sphere when the system is in specific entanglement while passing through the origin of the Bloch sphere when the system is in maximal entanglement.

level $|e\rangle$, the Hamiltonian of the individual qubit is given by $H_n = -i\gamma_n/2|e\rangle_n\langle e| + \Omega_n\sigma_n^x$, where γ_n and Ω_n are the decay rate and drive amplitude, respectively with the n -th qubit operators $\sigma_n^+ = |e\rangle_n\langle g|$, $\sigma_n^- = |g\rangle_n\langle e|$, $\sigma_n^x = |e\rangle_n\langle g| + |g\rangle_n\langle e|$. Its two eigenvalues are $E_{\pm} = -i\gamma_n/4 \pm 1/4\sqrt{-\gamma_n^2 + 16\Omega_n^2}$, featuring an EP at $\Omega_n = \gamma_n/4$. Conventionally, the post-selection or renormalizing states are involved in evaluating the performance of the system during the entanglement preparations for non-Hermitian systems. However, these method fails to account for a crucial factor, i.e., the success rate, which is of course very important for all practical applications. Here we define the success rate as

$$S = |\langle\psi_f|\psi_i\rangle|^2, \quad (2)$$

where $|\psi_i\rangle$ is the ideal maximal entanglement and $|\psi_f\rangle$ is the practical final state without normalization, the system evolution state can be written as

$$|\psi(t)\rangle = \sum_n c_n e^{-it \operatorname{Re}(E_n)} e^{t \operatorname{Im}(E_n)} |E_n\rangle,$$

in which E_n and $|E_n\rangle$ are eigenvalues and eigenstates of the system, respectively and c_n is the coefficient determined by the initial state. It can be seen that the imaginary part $\operatorname{Im}(E_n)$ will cause the probability amplitude to attenuate or amplify exponentially with time, while the real part $\operatorname{Re}(E_n)$ causes the state to oscillate [78]. For the all lossy EP system, the preparation of high-degree entanglement requires a relatively long evolution time and the

presence of negative imaginary components in the eigenvalue significantly decreases the probability amplitude of the evolution state, thus correspondingly leading to a low success rate. This highlights a critical phenomenon: the enhancement of entanglement is accompanied by a concomitant exponential decrement in the success rate, thus illustrating a distinct trade-off relation between the concurrence and success rate, as shown in Fig. 1(b), the success rate is negligible for the high-degree entanglement.

For preparing maximal or specific entanglement, numerical simulation methods are used to identify the optimal parameters $\{\Omega, t\}$ for preparing the desired entanglement in the shortest possible time. To have a deeper physical insight into optimal parameter selection and entanglement preparation, we analyze the dynamic trajectory of the reduced single qubit (after tracing out surplus qubits) [79], as illustrated in Fig. 1(c) and (d), the maximal (specific) entanglement can typically be prepared within a single cycle for systems with a small number of qubits. However, as the number of qubits increases, both the optimal parameters Ω and t increase, necessitating multi-cycle dynamics for the reduced single qubit.

To improve the success rate, we introduce the gain into the system, the Hamiltonian of the system is similar to Eq. (1) but with the single-qubit Hamiltonian H_n changed as

$$H'_n = -i\gamma_n/2|e\rangle\langle e| + i\kappa_n/2|g\rangle\langle g| + \Omega_n\sigma_n^x, \quad (3)$$

which has been realized in active \mathcal{PT} -devices. As the gain increases, the trade-off relation would be gradually broken, becoming entirely obsolete when the gain is balanced with the loss, facilitating the attainment of maximal entanglement with a high success rate. The primary reason is that the lost energy can be effectively compensated for the truly \mathcal{PT} -symmetric system, which enables the system's properties to resemble those of the closed system, thereby potentially improving the success rate of entanglement preparation with faster speed.

III. FAST \mathcal{PT} -SYMMETRIC ENTANGLEMENT WITH HIGH SUCCESS RATE

To set the stage, we first consider the two-qubit system to show our main results and generalize it to the triplet system to show the universality of our scheme.

A. Two-qubit entanglement

For the two-qubit system depicted in Fig. 2(a), the Hamiltonian can be described by $H = \sum_{n=1}^2 H_n + J(\sigma_1^+ \sigma_2^- + \sigma_1^- \sigma_2^+)$, we first confine our analysis to the all lossy EP system and assume $\gamma_n = \gamma$, $\Omega_n = \Omega$ for simplicity. The coupling between qubits lifts the degeneracy of the system, reducing the two-qubit system from fourth-order EP ($J = 0$) to second-order EP. The real-to-complex spectral phase transition at EP is critical to

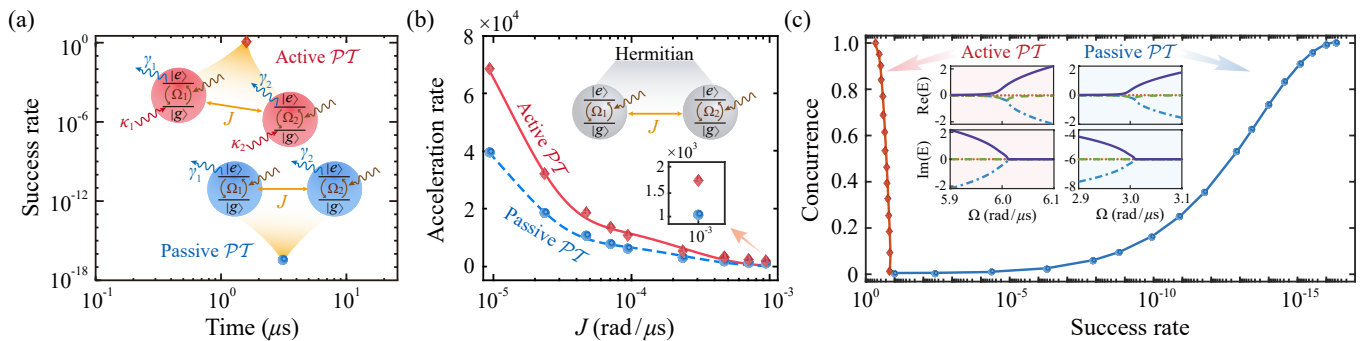


FIG. 2. (a) The duration required to prepare the maximal entanglement and the corresponding success rate for active and passive \mathcal{PT} -symmetric systems. (b) The acceleration rate, expressed as t_H/t , characterizes the acceleration effect of both active and passive \mathcal{PT} -symmetric systems across different coupling strengths. Here, t signifies the time required to achieve the maximal entanglement for passive or active schemes, and t_H denotes the corresponding duration for the Hermitian system. Ω of the Hermitian system is set the same as the active system. (c) The maximum concurrence limit is attainable under varying success rates for active and passive \mathcal{PT} -symmetric systems. Inset: The real and imaginary of the eigenvalues for both the active and passive \mathcal{PT} -symmetric systems, respectively. The initial state is $|gg\rangle$. $\gamma_{1(2)} = \kappa_{1(2)} = 12 \mu\text{s}^{-1}$, $J = 0.001 \text{ rad}/\mu\text{s}$ for Fig. (a) and (c). The optimal Ω to achieve maximal or specific concurrence is obtained numerically. In Fig. (a), the optimal Ω is found as $6.23 \text{ rad}/\mu\text{s}$ and $3.152 \text{ rad}/\mu\text{s}$ for active and passive \mathcal{PT} -symmetric systems, respectively.

improve the concurrence [21], which is useful for the evaluation of entanglement degree [80].

In comparison to Hermitian systems requiring significant durations (inversely proportional to qubit coupling) to prepare the maximal entanglement, non-Hermitian systems can greatly accelerate this process [21]. The acceleration rate for preparing the maximal entanglement under different coupling strengths is shown in Fig. 2(b) (blue dots), showing a reduction of the time duration by four orders of magnitude compared with Hermitian systems ($\gamma = 0$).

To quantify the success rate of entanglement preparation, Fig. 2(c) is the relation between the maximum concurrence limit and success rate for active and passive \mathcal{PT} -symmetric systems, note that to better observe the entanglement characteristics of the system (independent of the success rate), the final state is normalized before calculating the concurrence [21]. This visualization highlights a distinct trade-off between the concurrence and success rate for the passive \mathcal{PT} -symmetric system. However, this trade-off relation can be effectively broken by the truly \mathcal{PT} -symmetric system, preparing the high-degree entanglement with a high success rate. For the preparation of maximal entanglement, Fig. 2(a) illustrates the success rate and time required of truly \mathcal{PT} -symmetric and all lossy systems, the success rate is approximately 10^{-17} for the all lossy system, which is negligible, but the truly \mathcal{PT} -symmetric system led to a significant enhancement in the success rate, which is close to unity. Furthermore, it also exhibited a further acceleration effect compared with all lossy EP scenarios for the maximal entanglement (red diamonds), as shown in Fig. 2(b).

To further reveal the reasons behind the aforementioned results of truly \mathcal{PT} -symmetric system, we consider a gain factor κ_n in the ground state, assuming $\kappa_n = \kappa = \gamma_n = \gamma$, the eigenvalues of single qubit Hamil-

tonian shown in Eq. (3) are given by $\pm 1/2\sqrt{-\gamma^2 + 4\Omega^2}$, and the system becomes a truly \mathcal{PT} -symmetric system. For the two-qubit system, as shown in the inset in Fig. 2(c), when the drive amplitude is small ($\Omega < \gamma/2$), the gain is unable to compensate for the loss, the system is non-equilibrium, one of the eigenmodes undergoes exponential decay while another amplifies, with the remaining eigenmodes unchanged with time [65, 81]. Conversely, within the \mathcal{PT} -symmetric phase ($\Omega > \gamma/2$), the gain can fully compensate for the loss, stabilizing the system at the real eigenfrequency, the system behaves like the closed system [65, 81]. In contrast, the passive \mathcal{PT} -symmetric system, regardless of the magnitude of the driving amplitude, is incapable of counterbalancing the effect of loss, leading consistently to imaginary eigenvalues. Consequently, this underscores the potential of the truly \mathcal{PT} -symmetric system to boost the success rate of entanglement preparation significantly.

Fig. 3(a) illustrates how to identify the optimal parameters $\{\Omega, t\}$ to maximize the concurrence in the shortest possible time. Under the premise of achieving optimal success rate shown in Fig. 2(c), the optimal parameters we choose correspond to $\{6.23 \text{ rad}/\mu\text{s}, 1.8 \mu\text{s}\}$. With the increase of Ω , the maximal entanglement can still be prepared by prolonging the evolution time. Fig. 3(b) shows the upper limit of concurrence can be achieved under different given Ω , the entanglement always remains minimal and almost zero in the \mathcal{PT} -broken phase, upon entering the \mathcal{PT} -symmetric phase with increasing Ω , the maximal concurrence can be reached gradually and there always exists the maximal entanglement with further increase the Ω . The entanglement prepared in the \mathcal{PT} -symmetry broken region is steady-state entanglement (see Appendix A).

To get more physical intuition of the improvement in success rate, we here consider the impact of unbalanced gain-loss on the entanglement preparation. It should be

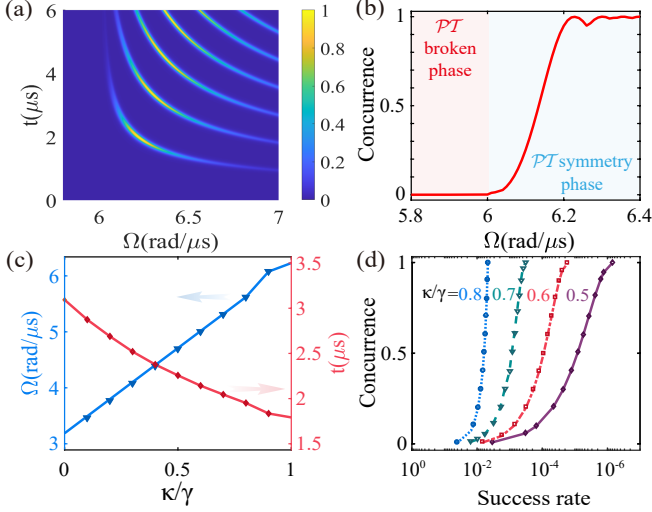


FIG. 3. (a) The evolution of concurrence with the driven amplitude Ω . (b) The upper bound of the concurrence under different Ω . (c) The optimal parameters for preparing the maximal entanglement in different ratios of gain-loss. (d) The upper bound of the concurrence with different success rates under the unbalanced gain-loss. Set $\gamma = 12 \mu\text{s}^{-1}$ for unbalanced gain-loss.

noted that for the preparation of maximal entanglement, the optimal parameters are different for different ratios of gain-loss, which is shown in Fig. 3(c). It is evident that the duration correspondingly extends as the discrepancy between gain and loss amplifies, which will decline the success rate as the negative eigenvalue's effect accumulates over time. The upper bound of the concurrence under different success rates is depicted in Fig. 3(d). It is observable that as the discrepancy of gain-loss increases, the success rate of preparing maximal entanglement decreases exponentially. For a certain gain, it can be seen that there still exists a trade-off relation, and as the discrepancy between gain and loss decreases, this relation gradually breaks down, the truly \mathcal{PT} -symmetric system is optimal for the preparation of maximal entanglement. In addition, the success rate is relatively high when the ratio κ/γ is greater than 0.8, which indicates the experimental requirements of our scheme can be relaxed.

To obtain the analytical result, we employ the first-order perturbation theory, treating the weak interaction Hamiltonian $H = J(\sigma_1^+ \sigma_2^- + \sigma_1^- \sigma_2^+)$ as a perturbation, thereby calculating the concurrence. By projecting the evolution state onto the perturbed eigenstate $|\psi(t)\rangle = \sum_{j=1}^4 \langle \Psi_j' | \psi_0 \rangle e^{-it\Lambda_j} | \Psi_j \rangle$, with $\langle \Psi_j' |$ denotes the left eigenstate within the biorthogonal basis and normalizing the evolution state, the concurrence can be obtained

$$C = 2 \frac{|A|}{B}, \quad (4)$$

which agrees well with the numerical findings. We give the specific calculation process and numerical result in Appendix A. With the optimal parameters, the form of the maximal entangled state $|\psi_f\rangle$ after normalization is

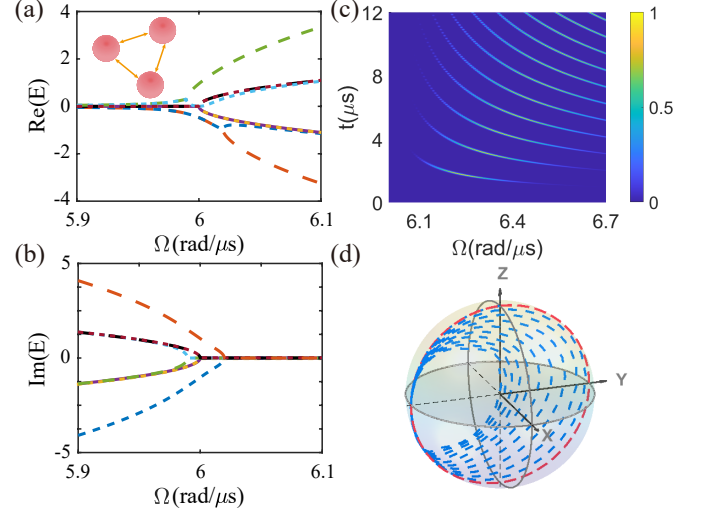


FIG. 4. Real (a) and imaginary (b) parts of the eigenvalues for the truly \mathcal{PT} -symmetric system. Inset in (a): the schematic diagram to prepare the triplet entanglement. (c) The residual tangle as a function of the driven amplitude and evolution time, identifying the maximum entanglement yields the optimal parameter $\{\Omega, t\} = \{6.58 \text{ rad}/\mu\text{s}, 11.57 \mu\text{s}\}$. (d) The dynamic trajectory of reduced single qubit on the Bloch sphere for the unperturbed system ($J = 0 \text{ rad}/\mu\text{s}$) (red) and perturbed system ($J = 0.001 \text{ rad}/\mu\text{s}$) (blue). The initial state is $|ggg\rangle$ and the other parameters are $J = 0.001 \text{ rad}/\mu\text{s}$ and $\kappa = \gamma = 12 \mu\text{s}^{-1}$.

exactly $|\psi_i\rangle$, which corresponds to the Bell state through a single-qubit Hadamard operation.

B. Triplet entanglement

To demonstrate the generality of the above theory, we now investigate the \mathcal{PT} symmetry improved triplet entanglement [see the inset in Fig. 4(a)]. The Hamiltonian is $H = \sum_{n=1}^3 H_n(H_n') + J \sum_{n \neq m=1}^3 \sigma_n^+ \sigma_m^-$ for triplet passive (active) \mathcal{PT} -symmetric system. It can be seen from the energy spectrum in Fig. 4(a) and (b) that the weak coupling between qubits lifts the degeneracy of the system, reducing from the eighth-order ($J = 0$) to fourth- and second-order EPs, the entanglement is also almost zero in the \mathcal{PT} -broken region. The normalized evolutionary state of the system is written as $|\psi'\rangle = |\psi\rangle/|\|\psi\rangle| = a_1|ggg\rangle + a_2|gge\rangle + a_3|geg\rangle + a_4|gee\rangle + a_5|egg\rangle + a_6|ege\rangle + a_7|eeg\rangle + a_8|eee\rangle$. To quantify the genuine three-body entanglement, the residual tangle $\tau_3 = C_{A|BC}^2 - C_{AB}^2 - C_{BC}^2$ is introduced [82], where $C_{AB(C)}^2$ quantifies the entanglement between qubits A and $B(C)$, $C_{A|BC}^2$ quantifies the qubit A and composite qubit system BC , which can be further expressed as [83]

$$\tau_3 = 4|d_1 - 2d_2 + 4d_3|, \quad (5)$$

where $d_1 = a_1^2 a_8^2 + a_2^2 a_7^2 + a_3^2 a_6^2 + a_4^2 a_5^2$, $d_2 = a_1 a_8 a_4 a_5 + a_1 a_8 a_3 a_6 + a_1 a_8 a_2 a_7 + a_3 a_4 a_5 a_6 + a_4 a_5 a_2 a_7 + a_2 a_7 a_3 a_6$

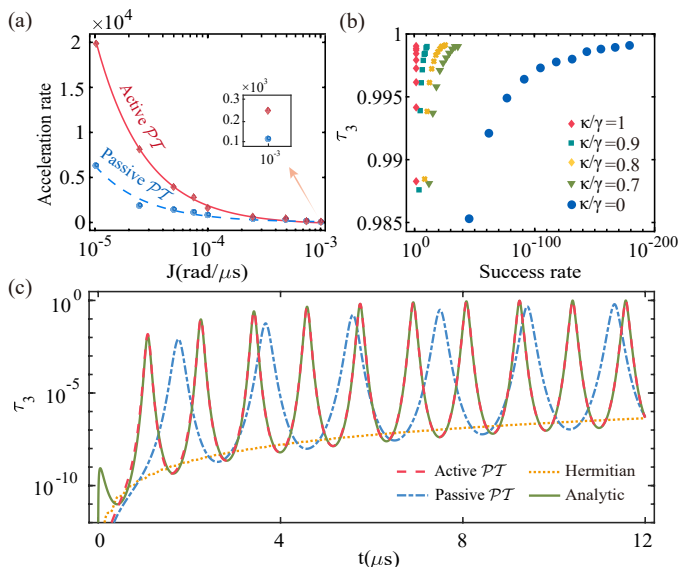


FIG. 5. (a) The acceleration rate of the active and passive \mathcal{PT} -symmetric systems. (b) The extremum of residual tangle τ_3 with respect to success rate. One can see the trade-off relation between τ_3 and the success rate for passive \mathcal{PT} -symmetric system ($\kappa/\gamma = 0$), which is significantly released for the unbalanced cases ($\kappa/\gamma = 0.7, 0.8, 0.9$) and totally broken for active \mathcal{PT} -symmetric system ($\kappa/\gamma = 1$). (c) The evolution of τ_3 for active, passive \mathcal{PT} -symmetric, and Hermitian systems. The green line shows the analytic result calculated by perturbation theory for the truly \mathcal{PT} -symmetric Hamiltonian. The optimal Ω is found numerically as 3.42 rad/ μ s for the all lossy EP system (Appendix B).

and $d_3 = a_1 a_7 a_4 a_6 + a_2 a_8 a_3 a_5$. Through solving the Schrödinger equation, we can get the success rate and τ_3 numerically.

We first briefly illustrate the preparation process of triplet entanglement for the truly \mathcal{PT} -symmetric system. The optimal parameter for a given coupling strength J is identified from Fig. 4(c). For a more intuitive understanding of entanglement preparation, we present the dynamic trajectory of reduced single qubit on the Bloch sphere in Fig. 4(d). In the absence of coupling between qubits, i.e., $J = 0$ rad/ μ s, the three qubits evolve independently. The reduced single qubit consistently evolves along the surface of the Bloch sphere, indicating the absence of entanglement among the three qubits. The system state evolves successively through $|ggg\rangle \rightarrow \bigotimes_{n=1,2,3} 1/\sqrt{2}(|g\rangle - i|e\rangle)_n \rightarrow |eee\rangle \rightarrow \bigotimes_{n=1,2,3} 1/\sqrt{2}(|g\rangle + i|e\rangle)_n \rightarrow |ggg\rangle$. Conversely, the weak inter-qubit coupling leads to imperfect dynamic evolution, preventing a complete return to the initial state within each periodic cycle (see Appendix B for detailed discussion), and the reduced single qubit gradually evolves into the inside of the Bloch sphere, demonstrating the system is in an entangled state. Furthermore, the evolution trajectory progressively deviates from the state $1/\sqrt{2}(|g\rangle + i|e\rangle)$ over successive cycles, eventually crossing the origin of the Bloch sphere, combining with unity for τ_3 , indicating that the system is in maximal entan-

glement.

The passive \mathcal{PT} -symmetric system has three orders of magnitude acceleration compared with the conventional Hermitian system, as shown in Fig. 5(a). However, the corresponding success rate approximates 10^{-180} for the preparation of maximal entanglement [depicted in Fig. 5(b)], which is negligible practically. Here we should stress that several cycles are considered to choose the optimal parameters corresponding to high-degree entanglement with τ_3 close to unity (Appendix B). We analyze numerically the value of τ_3 concerning the drive amplitude and evolution time and give that the upper bound of entanglement corresponds to different drive amplitude, which exhibits an oscillatory increasing trend with respect to the success rates (see Appendix B for details). Here we focus on the preparation of maximal entanglement, hence only the extremum points of τ_3 are presented in Fig. 5(b), there exists a trade-off relation between the entanglement and success rate.

For the truly \mathcal{PT} -symmetric system, as illustrated in Fig. 5(b) (depicted by the red diamonds), it can break the trade-off relation between the degree of entanglement and the success rate. Moreover, there is a further acceleration effect compared with the passive \mathcal{PT} -symmetric system, as evidenced by red diamonds in Fig. 5(a).

Considering the scenarios of unbalanced gain-loss, as shown in Fig. 5(b), one can observe that as the ratio of gain-loss increases, the trade-off relationship gradually breaks down, the success rate of achieving the same degree of entanglement correspondence increases exponentially. When the ratio of gain to loss falls below 0.8, achieving the maximal entanglement becomes impossible. Therefore, maintaining a balance between gain and loss is crucial for the preparation of high-degree entanglement with a high success rate.

Under eigenvalues Λ_j and eigenstates $|\Psi_j\rangle$ solved through the perturbation theory, the system state can be represented as $|\psi(t)\rangle = \sum_{j=1}^8 \langle \Psi_j | \psi_0 \rangle e^{-it\Lambda_j} |\Psi_j\rangle$. Assuming the initial state $|\psi_0\rangle$ is $|ggg\rangle$, the evolution of entanglement can be obtained

$$\tau_3 = \left| \frac{A}{4\eta^{12}B^2} \right|. \quad (6)$$

The specific calculation process is in Appendix B. From Fig. 5(c), we can see the perturbation analytic result is in good agreement with the numerical simulation result. Furthermore, it exhibits that the attainment of maximal entanglement is undergoing several Rabi-like cycles within the three-qubit system. Notably, the truly \mathcal{PT} -symmetric system exhibits a distinct acceleration effect compared with the all lossy and Hermitian systems.

IV. DISCUSSION

As the coupling strength is reduced, the time required to achieve maximal entanglement is extended for both Hermitian and non-Hermitian dynamics. However, the acceleration factor of truly \mathcal{PT} -symmetric sys-

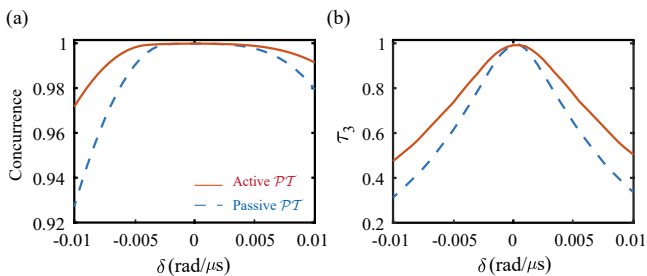


FIG. 6. The entanglement degree variation of bipartite (a) and tripartite (b) systems with respect to the non-resonant driving error. The optimal parameters are the same as Fig. 2 and Fig. 5, respectively.

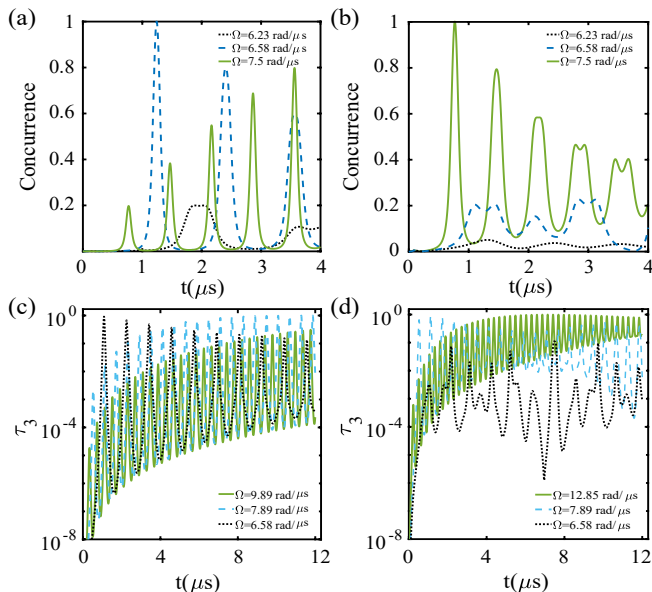


FIG. 7. The evolution of the concurrence for strong coupling $J = 0.01$ rad/ μ s (a) and $J = 0.1$ rad/ μ s (b), and residual tangle for coupling $J = 0.01$ rad/ μ s (c) and $J = 0.1$ rad/ μ s (d) under different driving amplitudes.

tem shows further improved, as illustrated in Fig. 2(b) and Fig. 5(a). In addition to significantly enhancing the success rate by multiple orders of magnitude, we investigate the influence of off-resonant driving effects. Specifically, considering the Hamiltonians of passive and truly \mathcal{PT} -symmetric qubits under error, they are represented as $H'_n = -i\gamma_n/2|e\rangle_n\langle e| + \delta_n|g\rangle_n\langle g| + \Omega_n\sigma_n^x$ and $H_n = -i\gamma_n/2|e\rangle_n\langle e| + (\kappa_n + \delta_n)|g\rangle_n\langle g| + \Omega_n\sigma_n^x$, respectively. For simplicity, we assume that the off-resonance error on the three qubits is the same, i.e., $\delta_n = \delta$. The active \mathcal{PT} -symmetric system demonstrates a remarkable resilience to the non-resonant error compared to the

all lossy case [see Fig. 6]. This resilience is likely attributed to the shorter operational duration, which results in reduced error accumulation. Moreover, when the coupling strength between qubits is much greater than $J = 0.001$ rad/ μ s, the maximal entanglement can still be prepared by appropriately selecting the driving amplitudes, accompanied by a noticeable acceleration effect compared to conventional Hermitian systems, as shown in Fig. 7. Additionally, satisfying the condition $4\Omega_1^2 - \gamma_1^2 = 4\Omega_2^2 - \gamma_2^2 = 4\Omega_3^2 - \gamma_3^2$ preserves a high degree of entanglement and enhances the acceleration effect, thereby overcoming the challenge of maintaining identical parameters across all three qubits (see Appendix B). We note that if methods exist for quantifying n -qubit entanglement ($n \geq 4$), the enhanced entanglement preparation in truly \mathcal{PT} -symmetric systems may also be applicable.

V. CONCLUSIONS

Our study shows that the truly \mathcal{PT} -symmetric system can be employed to accelerate the preparation of multi-qubit entanglement by several orders of magnitude than the conventional Hermitian system. The trade-off relation between success rate and entanglement degree predicted by the passive \mathcal{PT} -symmetric system can be broken by the truly \mathcal{PT} -symmetric system. The main reason is attributed to the fact that the energy is conserved in the \mathcal{PT} -symmetric phase region of truly \mathcal{PT} -symmetric system. A detailed analysis was conducted on the influence of the unbalanced gain-loss on the preparation of the maximal entanglement. Our finding paves a new way for high-efficiency multi-qubit entanglement preparation and is meaningful for large-scale quantum computing.

ACKNOWLEDGEMENT

This work was supported by the National Key R&D Program of China (Grants No. 2022YFA1404500 and 2021YFA1400900), Cross-disciplinary Innovative Research Group Project of Henan Province (Grant No. 232300421004), the National Natural Science Foundation of China (Grants No. 12125406, 12274376, and 12074232). and a major science and technology project of Henan Province under Grant No. 221100210400, and the Natural Science Foundation of Henan Province under Grant No. 232300421075 and 212300410085. H.J. is supported by the NSFC (11935006), the Science and Technology Innovation Program of Hunan Province (Grant No. 2020RC4047), National Key R&D Program of China (No. 2024YFE0102400) and Hunan provincial major sci-tech program (2023ZJ1010).

APPENDIX A: TWO-QUBIT PERTURBATION THEORY FOR THE TRULY \mathcal{PT} -SYMMETRIC SYSTEM

For the non-Hermitian Hamiltonian, it is essential to construct biorthogonal basis vectors, we first illustrate the construction of biorthogonal basis vectors for the single qubit in Hilbert space and its dual space. The Hamiltonian of the single-qubit in active \mathcal{PT} -symmetric system is

$$H_n = -i\gamma_n/2|e\rangle\langle e| + i\kappa_n/2|g\rangle\langle g| + \Omega_n\sigma_n^x, \quad (\text{A1})$$

with $\kappa_n = \gamma_n = \gamma$, the eigenvalues and eigenstates are

$$\begin{aligned} E_{\pm} &= \pm 1/2\sqrt{-\gamma^2 + 4\Omega^2}, \\ |\psi_{\pm}\rangle &= \frac{1}{2\sqrt{2}\Omega} \begin{pmatrix} i\gamma \pm \sqrt{-\gamma^2 + 4\Omega^2} \\ 2\Omega \end{pmatrix}. \end{aligned} \quad (\text{A2})$$

To construct the biorthogonal basis, the Hamiltonian in the dual space of H_n needs to consider

$$H'_n = i\gamma_n/2|e\rangle\langle e| - i\kappa_n/2|g\rangle\langle g| + \Omega_n\sigma_n^x, \quad (\text{A3})$$

with the eigenvalues and eigenstates

$$\begin{aligned} E'_{\pm} &= \pm 1/2\sqrt{-\gamma^2 + 4\Omega^2}, \\ |\psi'_{\pm}\rangle &= \frac{1}{2\sqrt{2}\Omega} \begin{pmatrix} -i\gamma \pm \sqrt{-\gamma^2 + 4\Omega^2} \\ 2\Omega \end{pmatrix}. \end{aligned} \quad (\text{A4})$$

It is easy to see that $|\psi_{\pm}\rangle$ does not satisfy the orthogonality due to the non-Hermitian nature of the Hamiltonian, i.e., $\langle\psi_+|\psi_-\rangle \neq 0$, but with the dual Hamiltonian H'_n , there have $\langle\psi'_+|\psi_-\rangle = \langle\psi'_-|\psi_+\rangle = 0$, and the normalized biorthogonal eigenstates can be constructed $|\bar{\psi}_{\pm}\rangle = |\psi_{\pm}\rangle/\sqrt{\langle\psi'_{\pm}|\psi_{\pm}\rangle}$.

For the two-qubit non-Hermitian Hamiltonian without the coupling between qubits $H_0 = \sum_{n=1}^2 -i\gamma_n/2|e\rangle\langle e| + i\kappa_n/2|g\rangle\langle g| + \Omega_n\sigma_n^x$, suppose $\kappa_n = \gamma_n = \gamma$ and $\eta = \sqrt{-\gamma^2 + 4\Omega^2}$, the first two eigenvalues and the corresponding eigenstates are

$$\begin{aligned} E_{++} &= \eta, \quad E_{--} = -\eta, \\ |\psi_{++}\rangle &= |\psi_+\rangle|\psi_+\rangle = \frac{1}{8\Omega^2} \begin{pmatrix} (i\gamma + \eta)^2 \\ 2\Omega(i\gamma + \eta) \\ 2\Omega(i\gamma + \eta) \\ 4\Omega^2 \end{pmatrix}, \quad |\psi_{--}\rangle = |\psi_-\rangle|\psi_-\rangle = \frac{1}{8\Omega^2} \begin{pmatrix} (i\gamma - \eta)^2 \\ 2\Omega(i\gamma - \eta) \\ 2\Omega(i\gamma - \eta) \\ 4\Omega^2 \end{pmatrix}. \end{aligned} \quad (\text{A5})$$

In the dual space, the eigenvalues and eigenstates of the Hamiltonian $H'_0 = \sum_{n=1}^2 i\gamma_n/2|e\rangle\langle e| - i\kappa_n/2|g\rangle\langle g| + \Omega_n\sigma_n^x$ are

$$\begin{aligned} E'_{++} &= \eta, \quad E'_{--} = -\eta, \\ |\psi'_{++}\rangle &= |\psi'_+\rangle|\psi'_+\rangle = \frac{1}{8\Omega^2} \begin{pmatrix} (-i\gamma + \eta)^2 \\ 2\Omega(-i\gamma + \eta) \\ 2\Omega(-i\gamma + \eta) \\ 4\Omega^2 \end{pmatrix}, \quad |\psi'_{--}\rangle = |\psi'_-\rangle|\psi'_-\rangle = \frac{1}{8\Omega^2} \begin{pmatrix} (-i\gamma - \eta)^2 \\ 2\Omega(-i\gamma - \eta) \\ 2\Omega(-i\gamma - \eta) \\ 4\Omega^2 \end{pmatrix}. \end{aligned} \quad (\text{A6})$$

The corresponding normalized biorthogonal eigenstates can be constructed as $|\bar{\psi}_{++}\rangle = |\psi_{++}\rangle/\sqrt{\langle\psi'_{++}|\psi_{++}\rangle}$ and $|\bar{\psi}_{--}\rangle = |\psi_{--}\rangle/\sqrt{\langle\psi'_{--}|\psi_{--}\rangle}$.

The other two eigenvalues and eigenstates are given by

$$\begin{aligned} E_{+-} &= E_{-+} = 0, \\ |\psi_{+-}\rangle &= |\psi_+\rangle|\psi_-\rangle = \frac{1}{4\Omega} \begin{pmatrix} -2\Omega \\ i\gamma + \eta \\ i\gamma - \eta \\ 2\Omega \end{pmatrix}, \quad |\psi_{-+}\rangle = |\psi_-\rangle|\psi_+\rangle = \frac{1}{4\Omega} \begin{pmatrix} -2\Omega \\ i\gamma - \eta \\ i\gamma + \eta \\ 2\Omega \end{pmatrix}, \end{aligned} \quad (\text{A7})$$

Similarly, in the dual space, the corresponding eigenvalues and eigenstates are

$$E'_{+-} = E'_{-+} = 0, \\ |\psi'_{+-}\rangle = |\psi'_+\rangle|\psi'_-\rangle = \frac{1}{4\Omega} \begin{pmatrix} -2\Omega \\ -i\gamma + \eta \\ -i\gamma - \eta \\ 2\Omega \end{pmatrix}, \quad |\psi'_{-+}\rangle = |\psi'_-\rangle|\psi'_+\rangle = \frac{1}{4\Omega} \begin{pmatrix} -2\Omega \\ -i\gamma - \eta \\ -i\gamma + \eta \\ 2\Omega \end{pmatrix}, \quad (\text{A8})$$

the normalized biorthogonal basis are $|\bar{\psi}_{+-}\rangle = |\psi_{+-}\rangle/\sqrt{\langle\psi'_{+-}|\psi_{+-}\rangle}$ and $|\bar{\psi}_{-+}\rangle = |\psi_{-+}\rangle/\sqrt{\langle\psi'_{-+}|\psi_{-+}\rangle}$.

At this point, we have constructed a complete set of biorthogonal basis of the Hamiltonian H_0 , including $\{|\bar{\psi}_{++}\rangle, |\bar{\psi}_{--}\rangle, |\bar{\psi}_{+-}\rangle, |\bar{\psi}_{-+}\rangle\}$ and corresponding $\{|\bar{\psi}'_{++}\rangle, |\bar{\psi}'_{--}\rangle, |\bar{\psi}'_{+-}\rangle, |\bar{\psi}'_{-+}\rangle\}$ in the dual space. It can be verified that these eigenvectors are not only normalized but also orthogonal to each other.

Consider the interaction Hamiltonian $H_I = J(\sigma_1^+ \sigma_2^- + \sigma_1^- \sigma_2^+)$, which we treat as perturbation due to the weak coupling between qubits. Next, we use the degenerate and non-degenerate perturbation theory to solve the system eigenvalues and eigenstates.

First consider the perturbation theory in the degenerate subspace, the perturbation matrix can be written as

$$H_i = \begin{pmatrix} \langle\bar{\psi}'_{+-}|H_I|\bar{\psi}_{+-}\rangle & \langle\bar{\psi}'_{+-}|H_I|\bar{\psi}_{-+}\rangle \\ \langle\bar{\psi}'_{-+}|H_I|\bar{\psi}_{+-}\rangle & \langle\bar{\psi}'_{-+}|H_I|\bar{\psi}_{-+}\rangle \end{pmatrix} = \begin{pmatrix} \frac{2J\Omega^2}{\gamma^2 - 4\Omega^2} & \frac{J(\gamma^2 - 2\Omega^2)}{\gamma^2 - 4\Omega^2} \\ \frac{J(\gamma^2 - 2\Omega^2)}{\gamma^2 - 4\Omega^2} & \frac{2J\Omega^2}{\gamma^2 - 4\Omega^2} \end{pmatrix}. \quad (\text{A9})$$

The eigenvalues of this Hermitian matrix are $\lambda_1 = -J$ and $\lambda_2 = \frac{J\gamma^2}{\gamma^2 - 4\Omega^2}$, the corresponding eigenstates are $|\lambda_1\rangle = (-|\bar{\psi}_{+-}\rangle + |\bar{\psi}_{-+}\rangle)/\sqrt{2}$, $|\lambda_2\rangle = (|\bar{\psi}_{+-}\rangle + |\bar{\psi}_{-+}\rangle)/\sqrt{2}$, which constructed a new set of basis vectors. In the dual space, the eigenstates are $|\lambda'_1\rangle = (-|\bar{\psi}'_{+-}\rangle + |\bar{\psi}'_{-+}\rangle)/\sqrt{2}$, $|\lambda'_2\rangle = (|\bar{\psi}'_{+-}\rangle + |\bar{\psi}'_{-+}\rangle)/\sqrt{2}$.

The first-order corrections for the eigenvalues are

$$\Lambda_1 = E_{+-} + \lambda_1 = -J, \\ \Lambda_2 = E_{-+} + \lambda_2 = \frac{J\gamma^2}{\gamma^2 - 4\Omega^2}, \quad (\text{A10})$$

and the perturbed eigenstates are given by

$$|\Psi_1\rangle = |\lambda_1\rangle + \frac{\langle\bar{\psi}'_{++}|H_I|\lambda_1\rangle}{E_{+-} - E_{++}}|\bar{\psi}_{++}\rangle + \frac{\langle\bar{\psi}'_{--}|H_I|\lambda_1\rangle}{E_{+-} - E_{--}}|\bar{\psi}_{--}\rangle, \\ |\Psi_2\rangle = |\lambda_2\rangle + \frac{\langle\bar{\psi}'_{++}|H_I|\lambda_2\rangle}{E_{-+} - E_{++}}|\bar{\psi}_{++}\rangle + \frac{\langle\bar{\psi}'_{--}|H_I|\lambda_2\rangle}{E_{-+} - E_{--}}|\bar{\psi}_{--}\rangle, \quad (\text{A11})$$

$$|\Psi'_1\rangle = |\lambda'_1\rangle + \frac{\langle\bar{\psi}_{++}|H_I|\lambda'_1\rangle}{E_{+-} - E_{++}}|\bar{\psi}'_{++}\rangle + \frac{\langle\bar{\psi}_{--}|H_I|\lambda'_1\rangle}{E_{+-} - E_{--}}|\bar{\psi}'_{--}\rangle, \\ |\Psi'_2\rangle = |\lambda'_2\rangle + \frac{\langle\bar{\psi}_{++}|H_I|\lambda'_2\rangle}{E_{-+} - E_{++}}|\bar{\psi}'_{++}\rangle + \frac{\langle\bar{\psi}_{--}|H_I|\lambda'_2\rangle}{E_{-+} - E_{--}}|\bar{\psi}'_{--}\rangle. \quad (\text{A12})$$

For non-degenerate subspace, the perturbation eigenvalue is obtained by using the first-order non-degenerate perturbation approximation

$$\Lambda_3 = E_{++} + \langle\bar{\psi}'_{++}|H_I|\psi'_{++}\rangle = \eta - \frac{2J\Omega^2}{\eta^2}, \\ \Lambda_4 = E_{--} + \langle\bar{\psi}'_{--}|H_I|\psi'_{--}\rangle = -\eta - \frac{2J\Omega^2}{\eta^2}, \quad (\text{A13})$$

the corresponding eigenstates are

$$|\Psi_3\rangle \approx |\bar{\psi}_{++}\rangle + \frac{\langle\bar{\psi}'_{--}|H_I|\bar{\psi}_{++}\rangle}{E_{++} - E_{--}}|\bar{\psi}_{--}\rangle,$$

$$|\Psi_4\rangle \approx |\bar{\psi}_{--}\rangle + \frac{\langle \bar{\psi}'_{++} | H_I | \bar{\psi}_{--} \rangle}{E_{--} - E_{++}} |\bar{\psi}_{++}\rangle. \quad (\text{A14})$$

$$|\Psi'_3\rangle \approx |\bar{\psi}'_{++}\rangle + \frac{\langle \bar{\psi}_{--} | H_I | \bar{\psi}'_{++} \rangle}{E_{++} - E_{--}} |\bar{\psi}_{--}\rangle,$$

$$|\Psi'_4\rangle \approx |\bar{\psi}'_{--}\rangle + \frac{\langle \bar{\psi}_{++} | H_I | \bar{\psi}'_{--} \rangle}{E_{--} - E_{++}} |\bar{\psi}_{++}\rangle. \quad (\text{A15})$$

At present, we have used perturbation theory to give the first-order corrected eigenvalues and eigenstates $\{|\Psi_1\rangle, |\Psi_2\rangle, |\Psi_3\rangle, |\Psi_4\rangle\}$ and $\{|\Psi'_1\rangle, |\Psi'_2\rangle, |\Psi'_3\rangle, |\Psi'_4\rangle\}$, these eigenvalues are not only normalized but also orthogonal to each other, thus can form a complete set of basis.

Assuming that the initial state of the system is $|\psi_0\rangle = |gg\rangle$, the system evolution state can be written as

$$\begin{aligned} |\psi(t)\rangle &= U(t)|\psi_0\rangle \\ &= U(t)(|\Psi_1\rangle\langle\Psi'_1| + |\Psi_2\rangle\langle\Psi'_2| + |\Psi_3\rangle\langle\Psi'_3| + |\Psi_4\rangle\langle\Psi'_4|)|\psi_0\rangle \\ &= \langle\Psi'_1|\psi_0\rangle U(t)|\Psi_1\rangle + \langle\Psi'_2|\psi_0\rangle U(t)|\Psi_2\rangle + \langle\Psi'_3|\psi_0\rangle U(t)|\Psi_3\rangle + \langle\Psi'_4|\psi_0\rangle U(t)|\Psi_4\rangle \\ &= \langle\Psi'_1|\psi_0\rangle e^{-it\Lambda_1} |\Psi_1\rangle + \langle\Psi'_2|\psi_0\rangle e^{-it\Lambda_2} |\Psi_2\rangle + \langle\Psi'_3|\psi_0\rangle e^{-it\Lambda_3} |\Psi_3\rangle + \langle\Psi'_4|\psi_0\rangle e^{-it\Lambda_4} |\Psi_4\rangle. \end{aligned} \quad (\text{A16})$$

After substituting in the corresponding eigenvalues and eigenstates, the final state is $|\psi_f\rangle = a|gg\rangle + b(|ge\rangle + |eg\rangle) + c|ee\rangle$, where

$$\begin{aligned} a &= \frac{\Omega^2}{\eta^8} \left[2\eta^2 e^{\frac{iJ\gamma^2 t}{\eta^2}} (\eta^2 + iJ\gamma)^2 - \frac{\Omega^2 e^{-it(\eta + \frac{2J\Omega^2}{\eta^2})} (Js + 2\eta^3)^2}{2s} + \frac{\Omega^2 e^{it(\eta - \frac{2J\Omega^2}{\eta^2})} (Jz + 2\eta^3)^2}{2z} \right] \\ b &= \frac{\Omega}{4\eta^8} \left[4\gamma\eta^4 e^{\frac{iJt\gamma^2}{\eta^2}} (J\gamma - i\gamma^2) - \frac{2\Omega^2(2\eta^3 + Js)}{s} e^{-it(\frac{2J\Omega^2}{\eta^2} + \eta)} (p + \eta^4 - i\gamma J\Omega^2) + \frac{2\Omega^2(2\eta^3 + Jz)}{z} \right. \\ &\quad \left. e^{it(-\frac{2J\Omega^2}{\eta^2} + \eta)} (p - \eta^4 + i\gamma J\Omega^2) \right], \\ c &= \frac{-\Omega^2}{2\eta^8} \left[4\eta^2 e^{\frac{iJt\gamma^2}{\eta^2}} (\eta^4 + \gamma^2 J^2) + 2e^{-it(\frac{2J\Omega^2}{\eta^2} + \eta)} (q + l) + 2e^{it(-\frac{2J\Omega^2}{\eta^2} + \eta)} (q - l) \right], \end{aligned} \quad (\text{A17})$$

with $s = \gamma^2 - 2\Omega^2 + i\gamma\eta$, $z = -\gamma^2 + 2\Omega^2 + i\gamma\eta$, $p = \eta(i\gamma^3 - 4i\gamma\Omega^2 + J\Omega^2)$, $q = 48\gamma^2\Omega^4 - J^2\Omega^4 - 64\Omega^6 + \gamma^6 - 12\gamma^4\Omega^2$, $l = 8J\eta\Omega^4 - 6J\gamma^2\eta\Omega^2 + J\gamma^4\eta$.

The concurrence can be obtained by

$$C = \frac{2|ac - b^2|}{|a|^2 + 2|b|^2 + |d|^2} = 2\frac{|A|}{B}, \quad (\text{A18})$$

where

$$\begin{aligned} A &= \frac{\Omega^2}{2} e^{-\frac{2it(\eta^3 + 2J\Omega^2)}{\eta^2}} \left[-2e^{\frac{2it(-J\eta^2 + \eta^3 + 6J\Omega^2)}{\eta^2}} \eta^{12} + 2e^{2it\eta} (\eta^6 - J^2\Omega^4) (\eta^6 - J^2\Omega^4 + iJ\eta^4\gamma) + e^{4it\eta} J\eta^2 (-2\eta^7\Omega^2 + 4J\eta^4\Omega^4 \right. \\ &\quad \left. + J^2\eta\Omega^4(\eta^2 - 2\Omega^2) + iJ^2\eta^2\Omega^4\gamma + \eta^9 - i\eta^8\gamma) + J(2\eta^9\Omega^2 + 4J\eta^6\Omega^4 + 2J^2\eta^3\Omega^6 - J^2\eta^4\Omega^4(\eta - i\gamma) - \eta^{11} - i\eta^{10}\gamma) \right], \end{aligned} \quad (\text{A19})$$

$$\begin{aligned} B &= \frac{1}{\eta^2} [\eta^{12}(3\gamma^2 + \eta^2)\Omega^2 + 4\eta^{10}(J^2 + 3\eta^2)\Omega^4 + 6J^2\eta^6(\gamma^2 - 3\eta^2)\Omega^6 + 24J^2\eta^6\Omega^8 + J^4(\gamma^2 + \eta^2)\Omega^{10} + 4J^4\Omega^{12} + (\eta^4 + \\ &\quad \gamma^2\Omega^2 - 5\eta^2\Omega^2 + 4\Omega^4)(\eta^6 - J^2\Omega^4)^2 \cos(2t\eta) + 2\eta^6\Omega^2(-\gamma^2 + \eta^2 - 4\Omega^2)(\eta^3 + J\Omega^2)^2 \cos\left(t\frac{J\eta^2 - \eta^3 - 6J\Omega^2}{\eta^2}\right) + 2\eta^6 \\ &\quad \Omega^2(-\gamma^2 + \eta^2 - 4\Omega^2)(\eta^3 - J\Omega^2)^2 \cos\left(t\frac{J\eta^2 + \eta^3 - 6J\Omega^2}{\eta^2}\right) + \gamma\eta(\eta^2 - 4\Omega^2)(\eta^{12} - J^4\Omega^8) \sin(2t\eta) - 4\gamma\eta^7\Omega^2(\eta^6 - J^2 \\ &\quad \Omega^4) \sin\left(t\frac{J\eta^2 - \eta^3 - 6J\Omega^2}{\eta^2}\right) + 4\gamma\eta^7\Omega^2(\eta^6 - J^2\Omega^4) \sin\left(t\frac{J\eta^2 + \eta^3 - 6J\Omega^2}{\eta^2}\right)]. \end{aligned} \quad (\text{A20})$$

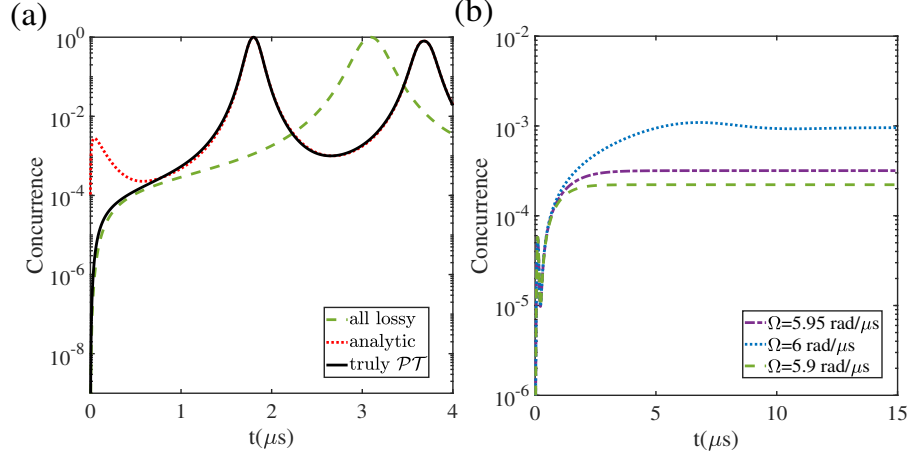


FIG. 8. (a) The evolution of concurrence for truly \mathcal{PT} -symmetric and all lossy systems with the analytic result calculated by the perturbation theory for the truly \mathcal{PT} -symmetric Hamiltonian, where $\Omega = 6.23$ rad/ μs and $\Omega = 3.152$ rad/ μs for truly \mathcal{PT} -symmetric and all lossy systems, respectively. (b) The evolution of concurrence in the \mathcal{PT} -broken phase for the truly \mathcal{PT} -symmetric system.

The analytical result is shown in Fig. 8(a), which agrees well with the numerical simulation result except for the region close to $t = 0$, and the truly \mathcal{PT} -symmetric system has an advantage in the speed of preparing the maximal entanglement. The form of the maximal entangled state before normalization is $|\psi_f\rangle = 0.3536e^{i5\pi/4}|ee\rangle + 0.3536e^{i\pi/4}(|ge\rangle + |eg\rangle + |gg\rangle)$, and is $(-|ee\rangle + |ge\rangle + |eg\rangle + |gg\rangle)/2$ after normalize, which correspond to the Bell state. In addition, we give the evolution of the concurrence in Fig. 8(b) in the \mathcal{PT} -broken phase for the truly \mathcal{PT} -symmetry Hamiltonian, the steady-state entanglement can be prepared, but the entanglement degree is really low.

APPENDIX B: TRIPLET MAXIMAL ENTANGLEMENT

1. Eigenvalues and eigenstates of the truly \mathcal{PT} -symmetric unperturbed Hamiltonian

Next, we demonstrate the triplet non-Hermitian Hamiltonian without the coupling between qubits $H_0 = \sum_{n=1}^3 i\kappa_n/2|g\rangle\langle g| - i\gamma_n/2|e\rangle\langle e| + \Omega_n\sigma_n^x$, with $\kappa_n = \gamma_n = \gamma$. The first two eigenvalues and the corresponding eigenstates are

$$E_{+++} = \frac{3\eta}{2}, \quad E_{---} = -\frac{3\eta}{2},$$

$$|\psi_{+++}\rangle = |\psi_+\rangle|\psi_+\rangle|\psi_+\rangle = \frac{1}{16\sqrt{2}\Omega^3} \begin{pmatrix} (i\gamma + \eta)^3 \\ 2\Omega(i\gamma + \eta)^2 \\ 2\Omega(i\gamma + \eta)^2 \\ 4\Omega^2(i\gamma + \eta) \\ 2\Omega(i\gamma + \eta)^2 \\ 4\Omega^2(i\gamma + \eta) \\ 4\Omega^2(i\gamma + \eta) \\ 8\Omega^3 \end{pmatrix}, \quad |\psi_{---}\rangle = |\psi_-\rangle|\psi_-\rangle|\psi_-\rangle = \frac{1}{16\sqrt{2}\Omega^3} \begin{pmatrix} -(-i\gamma + \eta)^3 \\ 2\Omega(-i\gamma + \eta)^2 \\ 2\Omega(-i\gamma + \eta)^2 \\ -4\Omega^2(-i\gamma + \eta) \\ 2\Omega(-i\gamma + \eta)^2 \\ -4\Omega^2(-i\gamma + \eta) \\ -4\Omega^2(-i\gamma + \eta) \\ 8\Omega^3 \end{pmatrix}. \quad (\text{B1})$$

Similarly, in the dual space, the eigenvalues and eigenstates of the Hamiltonian $H' = \sum_{n=1}^3 i\gamma_n/2|e\rangle\langle e| - i\kappa_n/2|g\rangle\langle g| + \Omega_n\sigma_n^x$ are

$$E'_{+++} = \frac{3\eta}{2}, \quad E'_{---} = -\frac{3\eta}{2},$$

$$|\psi'_{+++}\rangle = |\psi'_+\rangle|\psi'_+\rangle|\psi'_+\rangle = \frac{1}{16\sqrt{2}\Omega^3} \begin{pmatrix} (-i\gamma + \eta)^3 \\ 2\Omega(-i\gamma + \eta)^2 \\ 2\Omega(-i\gamma + \eta)^2 \\ 4\Omega^2(-i\gamma + \eta) \\ 2\Omega(-i\gamma + \eta)^2 \\ 4\Omega^2(-i\gamma + \eta) \\ 4\Omega^2(-i\gamma + \eta) \\ 8\Omega^3 \end{pmatrix}, \quad |\psi'_{---}\rangle = |\psi'_-\rangle|\psi'_-\rangle|\psi'_-\rangle = \frac{1}{16\sqrt{2}\Omega^3} \begin{pmatrix} -(i\gamma + \eta)^3 \\ 2\Omega(i\gamma + \eta)^2 \\ 2\Omega(i\gamma + \eta)^2 \\ -4\Omega^2(i\gamma + \eta) \\ 2\Omega(i\gamma + \eta)^2 \\ -4\Omega^2(i\gamma + \eta) \\ -4\Omega^2(i\gamma + \eta) \\ 8\Omega^3 \end{pmatrix}. \quad (\text{B2})$$

The corresponding normalized biorthogonal eigenstates can be constructed as $|\bar{\psi}_{+++}\rangle = |\psi_{+++}\rangle/\sqrt{\langle\psi'_{+++}|\psi_{+++}\rangle}$ and $|\bar{\psi}_{---}\rangle = |\psi_{---}\rangle/\sqrt{\langle\psi'_{---}|\psi_{---}\rangle}$.

The other three eigenvalues and eigenstates are given by

$$E_{+--} = E_{-+-} = E_{--+} = -\frac{\eta}{2},$$

$$|\psi_{+--}\rangle = |\psi_+\rangle|\psi_-\rangle|\psi_-\rangle = \frac{1}{8\sqrt{2}\Omega^2} \begin{pmatrix} 2\Omega(-i\gamma + \eta) \\ -4\Omega^2 \\ -4\Omega^2 \\ 2\Omega(i\gamma + \eta) \\ (-i\gamma + \eta)^2 \\ -2\Omega(-i\gamma + \eta) \\ -2\Omega(-i\gamma + \eta) \\ 4\Omega^2 \end{pmatrix}, \quad |\psi_{-+-}\rangle = |\psi_-\rangle|\psi_+\rangle|\psi_-\rangle = \frac{1}{8\sqrt{2}\Omega^2} \begin{pmatrix} 2\Omega(-i\gamma + \eta) \\ -4\Omega^2 \\ (-i\gamma + \eta)^2 \\ -2\Omega(-i\gamma + \eta) \\ -4\Omega^2 \\ 2\Omega(i\gamma + \eta) \\ -2\Omega(-i\gamma + \eta) \\ 4\Omega^2 \end{pmatrix},$$

$$|\psi_{--+}\rangle = |\psi_-\rangle|\psi_-\rangle|\psi_+\rangle = \frac{1}{8\sqrt{2}\Omega^2} \begin{pmatrix} 2\Omega(-i\gamma + \eta) \\ (-i\gamma + \eta)^2 \\ -4\Omega^2 \\ -2\Omega(-i\gamma + \eta) \\ -4\Omega^2 \\ -2\Omega(-i\gamma + \eta) \\ 2\Omega(i\gamma + \eta) \\ 4\Omega^2 \end{pmatrix}. \quad (\text{B3})$$

In the dual space, the corresponding eigenvalues and eigenstates are given by

$$E'_{+--} = E'_{-+-} = E'_{--+} = -\frac{\eta}{2},$$

$$|\psi'_{+--}\rangle = |\psi'_+\rangle|\psi'_-\rangle|\psi'_-\rangle = \frac{1}{8\sqrt{2}\Omega^2} \begin{pmatrix} 2\Omega(i\gamma + \eta) \\ -4\Omega^2 \\ -4\Omega^2 \\ 2\Omega(-i\gamma + \eta) \\ (i\gamma + \eta)^2 \\ -2\Omega(i\gamma + \eta) \\ -2\Omega(i\gamma + \eta) \\ 4\Omega^2 \end{pmatrix}, \quad |\psi'_{-+-}\rangle = |\psi'_-\rangle|\psi'_+\rangle|\psi'_-\rangle = \frac{1}{8\sqrt{2}\Omega^2} \begin{pmatrix} 2\Omega(i\gamma + \eta) \\ -4\Omega^2 \\ (i\gamma + \eta)^2 \\ -2\Omega(i\gamma + \eta) \\ -4\Omega^2 \\ 2\Omega(-i\gamma + \eta) \\ -2\Omega(i\gamma + \eta) \\ 4\Omega^2 \end{pmatrix},$$

$$|\psi'_{--+}\rangle = |\psi'_-\rangle|\psi'_-\rangle|\psi'_+\rangle = \frac{1}{8\sqrt{2}\Omega^2} \begin{pmatrix} 2\Omega(i\gamma + \eta) \\ (i\gamma + \eta)^2 \\ -4\Omega^2 \\ -2\Omega(i\gamma + \eta) \\ -4\Omega^2 \\ -2\Omega(i\gamma + \eta) \\ 2\Omega(-i\gamma + \eta) \\ 4\Omega^2 \end{pmatrix}. \quad (\text{B4})$$

Similarly, the normalized biorthogonal basis are $|\bar{\psi}_{+--}\rangle = |\psi_{+--}\rangle/\sqrt{\langle\psi'_{+--}|\psi_{+--}\rangle}$, $|\bar{\psi}_{-+-}\rangle = |\psi_{-+-}\rangle/\sqrt{\langle\psi'_{-+-}|\psi_{-+-}\rangle}$ and $|\bar{\psi}_{--+}\rangle = |\psi_{--+}\rangle/\sqrt{\langle\psi'_{--+}|\psi_{--+}\rangle}$.

And the last three eigenvalues and eigenstates are

$$\begin{aligned}
E_{-++} = E_{+-+} &= E_{+--} = \frac{\eta}{2}, \\
|\psi_{-++}\rangle = |\psi_{-}\rangle|\psi_{+}\rangle|\psi_{+}\rangle &= \frac{1}{8\sqrt{2}\Omega^2} \begin{pmatrix} -2\Omega(i\gamma + \eta) \\ -4\Omega^2 \\ -4\Omega^2 \\ -2\Omega(-i\gamma + \eta) \\ (i\gamma + \eta)^2 \\ 2\Omega(i\gamma + \eta) \\ 2\Omega(i\gamma + \eta) \\ 4\Omega^2 \end{pmatrix}, \quad |\psi_{+-+}\rangle = |\psi_{+}\rangle|\psi_{-}\rangle|\psi_{+}\rangle = \frac{1}{8\sqrt{2}\Omega^2} \begin{pmatrix} -2\Omega(i\gamma + \eta) \\ -4\Omega^2 \\ (i\gamma + \eta)^2 \\ 2\Omega(i\gamma + \eta) \\ -4\Omega^2 \\ -2\Omega(-i\gamma + \eta) \\ 2\Omega(i\gamma + \eta) \\ 4\Omega^2 \end{pmatrix}, \\
|\psi_{--+}\rangle = |\psi_{-}\rangle|\psi_{-}\rangle|\psi_{+}\rangle &= \frac{1}{8\sqrt{2}\Omega^2} \begin{pmatrix} -2\Omega(i\gamma + \eta) \\ (i\gamma + \eta)^2 \\ -4\Omega^2 \\ 2\Omega(i\gamma + \eta) \\ -4\Omega^2 \\ 2\Omega(i\gamma + \eta) \\ -2\Omega(-i\gamma + \eta) \\ 4\Omega^2 \end{pmatrix}, \tag{B5}
\end{aligned}$$

in the dual space, the eigenvalues and eigenstates are

$$\begin{aligned}
E'_{-++} = E'_{+-+} &= E'_{+--} = \frac{\eta}{2}, \\
|\psi'_{-++}\rangle = |\psi'_{-}\rangle|\psi'_{+}\rangle|\psi'_{+}\rangle &= \frac{1}{8\sqrt{2}\Omega^2} \begin{pmatrix} -2\Omega(-i\gamma + \eta) \\ -4\Omega^2 \\ -4\Omega^2 \\ -2\Omega(i\gamma + \eta) \\ (-i\gamma + \eta)^2 \\ 2\Omega(-i\gamma + \eta) \\ 2\Omega(-i\gamma + \eta) \\ 4\Omega^2 \end{pmatrix}, \quad |\psi'_{+-+}\rangle = |\psi'_{+}\rangle|\psi'_{-}\rangle|\psi'_{+}\rangle = \frac{1}{8\sqrt{2}\Omega^2} \begin{pmatrix} -2\Omega(-i\gamma + \eta) \\ -4\Omega^2 \\ (-i\gamma + \eta)^2 \\ 2\Omega(-i\gamma + \eta) \\ -4\Omega^2 \\ -2\Omega(i\gamma + \eta) \\ 2\Omega(-i\gamma + \eta) \\ 4\Omega^2 \end{pmatrix}, \\
|\psi'_{--+}\rangle = |\psi'_{-}\rangle|\psi'_{-}\rangle|\psi'_{+}\rangle &= \frac{1}{8\sqrt{2}\Omega^2} \begin{pmatrix} -2\Omega(-i\gamma + \eta) \\ (-i\gamma + \eta)^2 \\ -4\Omega^2 \\ 2\Omega(-i\gamma + \eta) \\ -4\Omega^2 \\ 2\Omega(-i\gamma + \eta) \\ -2\Omega(i\gamma + \eta) \\ 4\Omega^2 \end{pmatrix}, \tag{B6}
\end{aligned}$$

the normalized biorthogonal basis are $|\bar{\psi}_{-++}\rangle = |\psi_{-++}\rangle/\sqrt{\langle\psi'_{-++}|\psi_{-++}\rangle}$, $|\bar{\psi}_{--+}\rangle = |\psi_{--+}\rangle/\sqrt{\langle\psi'_{--+}|\psi_{--+}\rangle}$ and $|\bar{\psi}_{+-+}\rangle = |\psi_{+-+}\rangle/\sqrt{\langle\psi'_{+-+}|\psi_{+-+}\rangle}$.

At this point, we have constructed a complete set of orthogonal basis of the Hamiltonian H_0 , including normalized eigenvectors $\{|\bar{\psi}_{+++}\rangle, |\bar{\psi}_{---}\rangle, |\bar{\psi}_{+--}\rangle, |\bar{\psi}_{-+-}\rangle, |\bar{\psi}_{--+}\rangle, |\bar{\psi}_{-++}\rangle, |\bar{\psi}_{+-+}\rangle, |\bar{\psi}_{+-+}\rangle\}$ and corresponding normalized eigenvectors $\{|\bar{\psi}'_{+++}\rangle, |\bar{\psi}'_{---}\rangle, |\bar{\psi}'_{+--}\rangle, |\bar{\psi}'_{-+-}\rangle, |\bar{\psi}'_{--+}\rangle, |\bar{\psi}'_{-++}\rangle, |\bar{\psi}'_{+-+}\rangle, |\bar{\psi}'_{+-+}\rangle\}$ in the dual space. It is easily verified that these eigenvectors satisfy not only the normalization,

$$\begin{aligned}
\langle\bar{\psi}'_{+++}|\bar{\psi}_{+++}\rangle &= \langle\bar{\psi}'_{---}|\bar{\psi}_{---}\rangle = \langle\bar{\psi}'_{+--}|\bar{\psi}_{+--}\rangle = \langle\bar{\psi}'_{-+-}|\bar{\psi}_{-+-}\rangle \\
&= \langle\bar{\psi}'_{+--}|\bar{\psi}_{+--}\rangle = \langle\bar{\psi}'_{-+-}|\bar{\psi}_{-+-}\rangle = \langle\bar{\psi}'_{--+}\bar{\psi}_{--+}\rangle = \langle\bar{\psi}'_{+-+}|\bar{\psi}_{+-+}\rangle = 1, \tag{B7}
\end{aligned}$$

but also orthogonality,

$$\begin{aligned}
\langle\bar{\psi}'_{+++}|\bar{\psi}_{---}\rangle &= \langle\bar{\psi}'_{+++}|\bar{\psi}_{+--}\rangle = \langle\bar{\psi}'_{+++}|\bar{\psi}_{-+-}\rangle = \langle\bar{\psi}'_{+++}|\bar{\psi}_{--+}\rangle \\
&= \langle\bar{\psi}'_{+++}|\bar{\psi}_{-++}\rangle = \langle\bar{\psi}'_{+++}|\bar{\psi}_{+-+}\rangle = \langle\bar{\psi}'_{+++}|\bar{\psi}_{+-+}\rangle = 0, \\
\langle\bar{\psi}'_{---}|\bar{\psi}_{+++}\rangle &= \langle\bar{\psi}'_{---}|\bar{\psi}_{+--}\rangle = \langle\bar{\psi}'_{---}|\bar{\psi}_{-+-}\rangle = \langle\bar{\psi}'_{---}|\bar{\psi}_{--+}\rangle
\end{aligned}$$

$$= \langle \bar{\psi}'_{----} | \bar{\psi}_{-+++} \rangle = \langle \bar{\psi}'_{----} | \bar{\psi}_{+--+} \rangle = \langle \bar{\psi}'_{----} | \bar{\psi}_{+--+} \rangle = 0, \quad (\text{B8})$$

The remaining internal products of states are not shown here.

2. Degenerate and non-degenerate perturbation approximation

Since the coupling between qubits is very weak, we treat the interaction Hamiltonian $H_I = J \sum_{n \neq m=1}^3 \sigma_n^+ \sigma_m^-$ as a perturbation. Next, we consider using degenerate and non-degenerate perturbation theory to solve the eigenvalues and eigenstates of the system.

First consider perturbation theory in the degenerate case, for the first three degenerate states, the perturbation matrix can be written as

$$H_i^1 = \begin{pmatrix} \langle \bar{\psi}'_{+--} | H_I | \bar{\psi}_{+--} \rangle & \langle \bar{\psi}'_{+--} | H_I | \bar{\psi}_{-+-} \rangle & \langle \bar{\psi}'_{+--} | H_I | \bar{\psi}_{--+} \rangle \\ \langle \bar{\psi}'_{-+-} | H_I | \bar{\psi}_{+--} \rangle & \langle \bar{\psi}'_{-+-} | H_I | \bar{\psi}_{-+-} \rangle & \langle \bar{\psi}'_{-+-} | H_I | \bar{\psi}_{--+} \rangle \\ \langle \bar{\psi}'_{--+} | H_I | \bar{\psi}_{+--} \rangle & \langle \bar{\psi}'_{--+} | H_I | \bar{\psi}_{-+-} \rangle & \langle \bar{\psi}'_{--+} | H_I | \bar{\psi}_{--+} \rangle \end{pmatrix} = \begin{pmatrix} \frac{2J\Omega^2}{\gamma^2 - 4\Omega^2} & \frac{J(\gamma^2 - 2\Omega^2)}{\gamma^2 - 4\Omega^2} & \frac{J(\gamma^2 - 2\Omega^2)}{\gamma^2 - 4\Omega^2} \\ \frac{J(\gamma^2 - 2\Omega^2)}{\gamma^2 - 4\Omega^2} & \frac{2J\Omega^2}{\gamma^2 - 4\Omega^2} & \frac{J(\gamma^2 - 2\Omega^2)}{\gamma^2 - 4\Omega^2} \\ \frac{J(\gamma^2 - 2\Omega^2)}{\gamma^2 - 4\Omega^2} & \frac{J(\gamma^2 - 2\Omega^2)}{\gamma^2 - 4\Omega^2} & \frac{2J\Omega^2}{\gamma^2 - 4\Omega^2} \end{pmatrix}. \quad (\text{B9})$$

The eigenvalues of this Hermitian matrix are $\lambda_1 = \lambda_2 = -J$ and $\lambda_3 = \frac{2J(\gamma^2 - \Omega^2)}{\gamma^2 - 4\Omega^2}$ and the corresponding eigenstates are $|\lambda_1\rangle = (-|\bar{\psi}_{+--}\rangle + |\bar{\psi}_{-+-}\rangle)/\sqrt{2}$, $|\lambda_2\rangle = (-|\bar{\psi}_{+--}\rangle + 2|\bar{\psi}_{-+-}\rangle - |\bar{\psi}_{--+}\rangle)/\sqrt{6}$ and $|\lambda_3\rangle = (|\bar{\psi}_{+--}\rangle + |\bar{\psi}_{-+-}\rangle + |\bar{\psi}_{--+}\rangle)/\sqrt{3}$, which constructed a new set of basis vectors, and we have used Schmidt orthogonalization here. In the dual space, $|\lambda'_1\rangle = (-|\bar{\psi}'_{+--}\rangle + |\bar{\psi}'_{-+-}\rangle)/\sqrt{2}$, $|\lambda'_2\rangle = (-|\bar{\psi}'_{+--}\rangle + 2|\bar{\psi}'_{-+-}\rangle - |\bar{\psi}'_{--+}\rangle)/\sqrt{6}$ and $|\lambda'_3\rangle = (|\bar{\psi}'_{+--}\rangle + |\bar{\psi}'_{-+-}\rangle + |\bar{\psi}'_{--+}\rangle)/\sqrt{3}$.

Under the first-order non-degenerate perturbation theory, the perturbation eigenvalues are

$$\begin{aligned} \Lambda_1 &= E_{+--} + \lambda_1 = -\frac{\eta}{2} - J, \\ \Lambda_2 &= E_{-+-} + \lambda_2 = -\frac{\eta}{2} - J, \\ \Lambda_3 &= E_{--+} + \lambda_3 = -\frac{\eta}{2} + \frac{2J(\gamma^2 - \Omega^2)}{\gamma^2 - 4\Omega^2}. \end{aligned} \quad (\text{B10})$$

After the first-order correction of the eigenstate, the degenerate eigenstate becomes

$$\begin{aligned} |\Psi_1\rangle &= |\lambda_1\rangle + \frac{\langle \bar{\psi}'_{+++} | H_I | \lambda_1 \rangle}{E_{+--} - E_{+++}} |\bar{\psi}_{+++}\rangle + \frac{\langle \bar{\psi}'_{----} | H_I | \lambda_1 \rangle}{E_{+--} - E_{----}} |\bar{\psi}_{----}\rangle + \frac{\langle \bar{\psi}'_{--+} | H_I | \lambda_1 \rangle}{E_{+--} - E_{--+}} |\bar{\psi}_{--+}\rangle \\ &\quad + \frac{\langle \bar{\psi}'_{+-+} | H_I | \lambda_1 \rangle}{E_{+--} - E_{+-+}} |\bar{\psi}_{+-+}\rangle + \frac{\langle \bar{\psi}'_{++-} | H_I | \lambda_1 \rangle}{E_{+--} - E_{++-}} |\bar{\psi}_{++-}\rangle \approx |\lambda_1\rangle, \\ |\Psi_2\rangle &= |\lambda_2\rangle + \frac{\langle \bar{\psi}'_{+++} | H_I | \lambda_2 \rangle}{E_{-+-} - E_{+++}} |\bar{\psi}_{+++}\rangle + \frac{\langle \bar{\psi}'_{----} | H_I | \lambda_2 \rangle}{E_{-+-} - E_{----}} |\bar{\psi}_{----}\rangle + \frac{\langle \bar{\psi}'_{--+} | H_I | \lambda_2 \rangle}{E_{-+-} - E_{--+}} |\bar{\psi}_{--+}\rangle \\ &\quad + \frac{\langle \bar{\psi}'_{+-+} | H_I | \lambda_2 \rangle}{E_{-+-} - E_{+-+}} |\bar{\psi}_{+-+}\rangle + \frac{\langle \bar{\psi}'_{++-} | H_I | \lambda_2 \rangle}{E_{-+-} - E_{++-}} |\bar{\psi}_{++-}\rangle \approx |\lambda_2\rangle, \\ |\Psi_3\rangle &= |\lambda_3\rangle + \frac{\langle \bar{\psi}'_{+++} | H_I | \lambda_3 \rangle}{E_{--+} - E_{+++}} |\bar{\psi}_{+++}\rangle + \frac{\langle \bar{\psi}'_{----} | H_I | \lambda_3 \rangle}{E_{--+} - E_{----}} |\bar{\psi}_{----}\rangle + \frac{\langle \bar{\psi}'_{--+} | H_I | \lambda_3 \rangle}{E_{--+} - E_{--+}} |\bar{\psi}_{--+}\rangle \\ &\quad + \frac{\langle \bar{\psi}'_{+-+} | H_I | \lambda_3 \rangle}{E_{--+} - E_{+-+}} |\bar{\psi}_{+-+}\rangle + \frac{\langle \bar{\psi}'_{++-} | H_I | \lambda_3 \rangle}{E_{--+} - E_{++-}} |\bar{\psi}_{++-}\rangle \approx |\lambda_3\rangle, \quad (\text{B11}) \\ |\Psi'_1\rangle &= |\lambda'_1\rangle + \frac{\langle \bar{\psi}_{+++} | H_I | \lambda'_1 \rangle}{E_{+--} - E_{+++}} |\bar{\psi}'_{+++}\rangle + \frac{\langle \bar{\psi}_{----} | H_I | \lambda'_1 \rangle}{E_{+--} - E_{----}} |\bar{\psi}'_{----}\rangle + \frac{\langle \bar{\psi}_{--+} | H_I | \lambda'_1 \rangle}{E_{+--} - E_{--+}} |\bar{\psi}'_{--+}\rangle \\ &\quad + \frac{\langle \bar{\psi}_{+-+} | H_I | \lambda'_1 \rangle}{E_{+--} - E_{+-+}} |\bar{\psi}'_{+-+}\rangle + \frac{\langle \bar{\psi}_{++-} | H_I | \lambda'_1 \rangle}{E_{+--} - E_{++-}} |\bar{\psi}'_{++-}\rangle \approx |\lambda'_1\rangle, \end{aligned}$$

$$\begin{aligned}
|\Psi'_2\rangle &= |\lambda'_2\rangle + \frac{\langle\bar{\psi}_{+++}|H_I|\lambda'_2\rangle}{E_{-+-} - E_{+++}}|\bar{\psi}'_{+++}\rangle + \frac{\langle\bar{\psi}_{---}|H_I|\lambda'_2\rangle}{E_{-+-} - E_{---}}|\bar{\psi}'_{---}\rangle + \frac{\langle\bar{\psi}_{--+}|H_I|\lambda'_2\rangle}{E_{-+-} - E_{--+}}|\bar{\psi}'_{--+}\rangle \\
&\quad + \frac{\langle\bar{\psi}_{+-+}|H_I|\lambda'_2\rangle}{E_{-+-} - E_{+-+}}|\bar{\psi}'_{+-+}\rangle + \frac{\langle\bar{\psi}_{+--}|H_I|\lambda'_2\rangle}{E_{-+-} - E_{+--}}|\bar{\psi}'_{+--}\rangle \approx |\lambda'_2\rangle, \\
|\Psi'_3\rangle &= |\lambda'_3\rangle + \frac{\langle\bar{\psi}_{+++}|H_I|\lambda'_3\rangle}{E_{-+-} - E_{+++}}|\bar{\psi}'_{+++}\rangle + \frac{\langle\bar{\psi}_{---}|H_I|\lambda'_3\rangle}{E_{-+-} - E_{---}}|\bar{\psi}'_{---}\rangle + \frac{\langle\bar{\psi}_{--+}|H_I|\lambda'_3\rangle}{E_{-+-} - E_{--+}}|\bar{\psi}'_{--+}\rangle \\
&\quad + \frac{\langle\bar{\psi}_{+-+}|H_I|\lambda'_3\rangle}{E_{-+-} - E_{+-+}}|\bar{\psi}'_{+-+}\rangle + \frac{\langle\bar{\psi}_{+--}|H_I|\lambda'_3\rangle}{E_{-+-} - E_{+--}}|\bar{\psi}'_{+--}\rangle \approx |\lambda'_3\rangle.
\end{aligned} \tag{B12}$$

For the last three degenerate states, the perturbation matrix can be written as

$$H_i^2 = \begin{pmatrix} \langle\bar{\psi}'_{--+}|H_I|\bar{\psi}_{--+}\rangle & \langle\bar{\psi}'_{--+}|H_I|\bar{\psi}_{+-+}\rangle & \langle\bar{\psi}'_{--+}|H_I|\bar{\psi}_{+--}\rangle \\ \langle\bar{\psi}'_{+-+}|H_I|\bar{\psi}_{--+}\rangle & \langle\bar{\psi}'_{+-+}|H_I|\bar{\psi}_{+-+}\rangle & \langle\bar{\psi}'_{+-+}|H_I|\bar{\psi}_{+--}\rangle \\ \langle\bar{\psi}'_{+--}|H_I|\bar{\psi}_{--+}\rangle & \langle\bar{\psi}'_{+--}|H_I|\bar{\psi}_{+-+}\rangle & \langle\bar{\psi}'_{+--}|H_I|\bar{\psi}_{+--}\rangle \end{pmatrix} = \begin{pmatrix} \frac{2J\Omega^2}{\gamma^2-4\Omega^2} & \frac{J(\gamma^2-2\Omega^2)}{\gamma^2-4\Omega^2} & \frac{J(\gamma^2-2\Omega^2)}{\gamma^2-4\Omega^2} \\ \frac{J(\gamma^2-2\Omega^2)}{\gamma^2-4\Omega^2} & \frac{2J\Omega^2}{\gamma^2-4\Omega^2} & \frac{J(\gamma^2-2\Omega^2)}{\gamma^2-4\Omega^2} \\ \frac{J(\gamma^2-2\Omega^2)}{\gamma^2-4\Omega^2} & \frac{J(\gamma^2-2\Omega^2)}{\gamma^2-4\Omega^2} & \frac{2J\Omega^2}{\gamma^2-4\Omega^2} \end{pmatrix}. \tag{B13}$$

The eigenvalues of this Hermitian matrix are $\lambda_4 = \lambda_5 = -J$ and $\lambda_6 = \frac{2J(\gamma^2-\Omega^2)}{\gamma^2-4\Omega^2}$ and the corresponding eigenstates are $|\lambda_4\rangle = (-|\bar{\psi}_{--+}\rangle + |\bar{\psi}_{+-+}\rangle)/\sqrt{2}$, $|\lambda_5\rangle = (-|\bar{\psi}_{--+}\rangle + 2|\bar{\psi}_{+-+}\rangle - |\bar{\psi}_{+--}\rangle)/\sqrt{6}$ and $|\lambda_6\rangle = (|\bar{\psi}_{--+}\rangle + |\bar{\psi}_{+-+}\rangle + |\bar{\psi}_{+--}\rangle)/\sqrt{3}$, which constructed a new set of basis vectors. In the dual space, $|\lambda'_4\rangle = (-|\bar{\psi}'_{--+}\rangle + |\bar{\psi}'_{+-+}\rangle)/\sqrt{2}$, $|\lambda'_5\rangle = (-|\bar{\psi}'_{--+}\rangle + 2|\bar{\psi}'_{+-+}\rangle - |\bar{\psi}'_{+--}\rangle)/\sqrt{6}$ and $|\lambda'_6\rangle = (|\bar{\psi}'_{--+}\rangle + |\bar{\psi}'_{+-+}\rangle + |\bar{\psi}'_{+--}\rangle)/\sqrt{3}$.

Similarly, the perturbation eigenvalue are

$$\begin{aligned}
\Lambda_4 &= E_{-+-} + \lambda_4 = \frac{\eta}{2} - J, \\
\Lambda_5 &= E_{-+-} + \lambda_5 = \frac{\eta}{2} - J, \\
\Lambda_6 &= E_{-+-} + \lambda_6 = \frac{\eta}{2} + \frac{2J(\gamma^2 - \Omega^2)}{\gamma^2 - 4\Omega^2}.
\end{aligned} \tag{B14}$$

After the first-order correction of the eigenstate, the degenerate eigenstate becomes

$$\begin{aligned}
|\Psi_4\rangle &= |\lambda_4\rangle + \frac{\langle\bar{\psi}'_{+++}|H_I|\lambda_4\rangle}{E_{-+-} - E_{+++}}|\bar{\psi}_{+++}\rangle + \frac{\langle\bar{\psi}'_{---}|H_I|\lambda_4\rangle}{E_{-+-} - E_{---}}|\bar{\psi}_{---}\rangle + \frac{\langle\bar{\psi}'_{--+}|H_I|\lambda_4\rangle}{E_{-+-} - E_{--+}}|\bar{\psi}_{--+}\rangle \\
&\quad + \frac{\langle\bar{\psi}'_{+-+}|H_I|\lambda_4\rangle}{E_{-+-} - E_{+-+}}|\bar{\psi}_{+-+}\rangle + \frac{\langle\bar{\psi}'_{+--}|H_I|\lambda_4\rangle}{E_{-+-} - E_{+--}}|\bar{\psi}_{+--}\rangle \approx |\lambda_4\rangle, \\
|\Psi_5\rangle &= |\lambda_5\rangle + \frac{\langle\bar{\psi}'_{+++}|H_I|\lambda_5\rangle}{E_{-+-} - E_{+++}}|\bar{\psi}_{+++}\rangle + \frac{\langle\bar{\psi}'_{---}|H_I|\lambda_5\rangle}{E_{-+-} - E_{---}}|\bar{\psi}_{---}\rangle + \frac{\langle\bar{\psi}'_{--+}|H_I|\lambda_5\rangle}{E_{-+-} - E_{--+}}|\bar{\psi}_{--+}\rangle \\
&\quad + \frac{\langle\bar{\psi}'_{+-+}|H_I|\lambda_5\rangle}{E_{-+-} - E_{+-+}}|\bar{\psi}_{+-+}\rangle + \frac{\langle\bar{\psi}'_{+--}|H_I|\lambda_5\rangle}{E_{-+-} - E_{+--}}|\bar{\psi}_{+--}\rangle \approx |\lambda_5\rangle, \\
|\Psi_6\rangle &= |\lambda_6\rangle + \frac{\langle\bar{\psi}'_{+++}|H_I|\lambda_6\rangle}{E_{-+-} - E_{+++}}|\bar{\psi}_{+++}\rangle + \frac{\langle\bar{\psi}'_{---}|H_I|\lambda_6\rangle}{E_{-+-} - E_{---}}|\bar{\psi}_{---}\rangle + \frac{\langle\bar{\psi}'_{--+}|H_I|\lambda_6\rangle}{E_{-+-} - E_{--+}}|\bar{\psi}_{--+}\rangle \\
&\quad + \frac{\langle\bar{\psi}'_{+-+}|H_I|\lambda_6\rangle}{E_{-+-} - E_{+-+}}|\bar{\psi}_{+-+}\rangle + \frac{\langle\bar{\psi}'_{+--}|H_I|\lambda_6\rangle}{E_{-+-} - E_{+--}}|\bar{\psi}_{+--}\rangle \approx |\lambda_6\rangle, \\
|\Psi'_4\rangle &= |\lambda'_4\rangle + \frac{\langle\bar{\psi}_{+++}|H_I|\lambda'_4\rangle}{E_{-+-} - E_{+++}}|\bar{\psi}'_{+++}\rangle + \frac{\langle\bar{\psi}_{---}|H_I|\lambda'_4\rangle}{E_{-+-} - E_{---}}|\bar{\psi}'_{---}\rangle + \frac{\langle\bar{\psi}_{--+}|H_I|\lambda'_4\rangle}{E_{-+-} - E_{--+}}|\bar{\psi}'_{--+}\rangle \\
&\quad + \frac{\langle\bar{\psi}_{+-+}|H_I|\lambda'_4\rangle}{E_{-+-} - E_{+-+}}|\bar{\psi}'_{+-+}\rangle + \frac{\langle\bar{\psi}_{+--}|H_I|\lambda'_4\rangle}{E_{-+-} - E_{+--}}|\bar{\psi}'_{+--}\rangle \approx |\lambda'_4\rangle,
\end{aligned} \tag{B15}$$

$$\begin{aligned}
|\Psi'_5\rangle &= |\lambda'_5\rangle + \frac{\langle\bar{\psi}_{+++}|H_I|\lambda'_5\rangle}{E_{+++} - E_{++++}}|\bar{\psi}'_{+++}\rangle + \frac{\langle\bar{\psi}_{---}|H_I|\lambda'_5\rangle}{E_{+++} - E_{----}}|\bar{\psi}'_{---}\rangle + \frac{\langle\bar{\psi}_{+--}|H_I|\lambda'_5\rangle}{E_{+++} - E_{+--}}|\bar{\psi}'_{+--}\rangle \\
&\quad + \frac{\langle\bar{\psi}_{-+-}|H_I|\lambda'_5\rangle}{E_{+++} - E_{-+-}}|\bar{\psi}'_{-+-}\rangle + \frac{\langle\bar{\psi}_{--+}|H_I|\lambda'_5\rangle}{E_{+++} - E_{--+}}|\bar{\psi}'_{--+}\rangle \approx |\lambda'_5\rangle, \\
|\Psi'_6\rangle &= |\lambda'_6\rangle + \frac{\langle\bar{\psi}_{+++}|H_I|\lambda'_6\rangle}{E_{+++} - E_{++++}}|\bar{\psi}'_{+++}\rangle + \frac{\langle\bar{\psi}_{---}|H_I|\lambda'_6\rangle}{E_{+++} - E_{----}}|\bar{\psi}'_{---}\rangle + \frac{\langle\bar{\psi}_{+--}|H_I|\lambda'_6\rangle}{E_{+++} - E_{+--}}|\bar{\psi}'_{+--}\rangle \\
&\quad + \frac{\langle\bar{\psi}_{-+-}|H_I|\lambda'_6\rangle}{E_{+++} - E_{-+-}}|\bar{\psi}'_{-+-}\rangle + \frac{\langle\bar{\psi}_{--+}|H_I|\lambda'_6\rangle}{E_{+++} - E_{--+}}|\bar{\psi}'_{--+}\rangle \approx |\lambda'_6\rangle.
\end{aligned} \tag{B16}$$

For non-degenerate subspaces, the perturbation eigenvalue can be obtained by using the first-order non-degenerate perturbation approximation

$$\begin{aligned}
\Lambda_7 &= E_{+++} + \langle\bar{\psi}'_{+++}|H_I|\psi'_{+++}\rangle = \frac{3\eta}{2} - \frac{6J\Omega^2}{\gamma^2 - 4\Omega^2}, \\
\Lambda_8 &= E_{---} + \langle\bar{\psi}'_{---}|H_I|\psi'_{---}\rangle = -\frac{3\eta}{2} - \frac{6J\Omega^2}{\gamma^2 - 4\Omega^2}.
\end{aligned} \tag{B17}$$

The corresponding eigenstates are

$$\begin{aligned}
|\Psi_7\rangle &= |\bar{\psi}_{+++}\rangle + \frac{\langle\bar{\psi}'_{---}|H_I|\bar{\psi}_{+++}\rangle}{E_{+++} - E_{----}}|\bar{\psi}_{---}\rangle + \frac{\langle\bar{\psi}'_{+--}|H_I|\bar{\psi}_{+++}\rangle}{E_{+++} - E_{+--}}|\bar{\psi}_{+--}\rangle + \frac{\langle\bar{\psi}'_{-+-}|H_I|\bar{\psi}_{+++}\rangle}{E_{+++} - E_{-+-}}|\bar{\psi}_{-+-}\rangle \\
&\quad + \frac{\langle\bar{\psi}'_{--+}|H_I|\bar{\psi}_{+++}\rangle}{E_{+++} - E_{--+}}|\bar{\psi}_{--+}\rangle + \frac{\langle\bar{\psi}'_{+++}|H_I|\bar{\psi}_{+++}\rangle}{E_{+++} - E_{+++}}|\bar{\psi}_{+++}\rangle + \frac{\langle\bar{\psi}'_{+--}|H_I|\bar{\psi}_{+++}\rangle}{E_{+++} - E_{+--}}|\bar{\psi}_{+--}\rangle \\
&\quad + \frac{\langle\bar{\psi}'_{-+-}|H_I|\bar{\psi}_{+++}\rangle}{E_{+++} - E_{-+-}}|\bar{\psi}_{-+-}\rangle \approx |\lambda_7\rangle + \frac{\langle\bar{\psi}'_{---}|H_I|\bar{\psi}_{+++}\rangle}{E_{+++} - E_{----}}|\bar{\psi}_{---}\rangle, \\
|\Psi_8\rangle &= |\bar{\psi}_{---}\rangle + \frac{\langle\bar{\psi}'_{+++}|H_I|\bar{\psi}_{---}\rangle}{E_{---} - E_{++++}}|\bar{\psi}_{+++}\rangle + \frac{\langle\bar{\psi}'_{+--}|H_I|\bar{\psi}_{---}\rangle}{E_{---} - E_{+--}}|\bar{\psi}_{+--}\rangle + \frac{\langle\bar{\psi}'_{-+-}|H_I|\bar{\psi}_{---}\rangle}{E_{---} - E_{-+-}}|\bar{\psi}_{-+-}\rangle \\
&\quad + \frac{\langle\bar{\psi}'_{--+}|H_I|\bar{\psi}_{---}\rangle}{E_{---} - E_{--+}}|\bar{\psi}_{--+}\rangle + \frac{\langle\bar{\psi}'_{+++}|H_I|\bar{\psi}_{---}\rangle}{E_{---} - E_{+++}}|\bar{\psi}_{+++}\rangle + \frac{\langle\bar{\psi}'_{+--}|H_I|\bar{\psi}_{---}\rangle}{E_{---} - E_{+--}}|\bar{\psi}_{+--}\rangle \\
&\quad + \frac{\langle\bar{\psi}'_{-+-}|H_I|\bar{\psi}_{---}\rangle}{E_{---} - E_{-+-}}|\bar{\psi}_{-+-}\rangle \approx |\lambda_8\rangle + \frac{\langle\bar{\psi}'_{+++}|H_I|\bar{\psi}_{---}\rangle}{E_{---} - E_{++++}}|\bar{\psi}_{+++}\rangle, \\
|\Psi'_7\rangle &= |\bar{\psi}'_{+++}\rangle + \frac{\langle\bar{\psi}_{---}|H_I|\bar{\psi}'_{+++}\rangle}{E_{+++} - E_{----}}|\bar{\psi}'_{---}\rangle + \frac{\langle\bar{\psi}_{+--}|H_I|\bar{\psi}'_{+++}\rangle}{E_{+++} - E_{+--}}|\bar{\psi}'_{+--}\rangle + \frac{\langle\bar{\psi}_{-+-}|H_I|\bar{\psi}'_{+++}\rangle}{E_{+++} - E_{-+-}}|\bar{\psi}'_{-+-}\rangle \\
&\quad + \frac{\langle\bar{\psi}_{--+}|H_I|\bar{\psi}'_{+++}\rangle}{E_{+++} - E_{--+}}|\bar{\psi}'_{--+}\rangle + \frac{\langle\bar{\psi}_{+++}|H_I|\bar{\psi}'_{+++}\rangle}{E_{+++} - E_{+++}}|\bar{\psi}'_{+++}\rangle + \frac{\langle\bar{\psi}_{+--}|H_I|\bar{\psi}'_{+++}\rangle}{E_{+++} - E_{+--}}|\bar{\psi}'_{+--}\rangle \\
&\quad + \frac{\langle\bar{\psi}_{-+-}|H_I|\bar{\psi}'_{+++}\rangle}{E_{+++} - E_{-+-}}|\bar{\psi}'_{-+-}\rangle \approx |\lambda'_7\rangle + \frac{\langle\bar{\psi}_{---}|H_I|\bar{\psi}'_{+++}\rangle}{E_{+++} - E_{----}}|\bar{\psi}'_{---}\rangle, \\
|\Psi'_8\rangle &= |\bar{\psi}'_{---}\rangle + \frac{\langle\bar{\psi}_{+++}|H_I|\bar{\psi}'_{---}\rangle}{E_{---} - E_{++++}}|\bar{\psi}'_{+++}\rangle + \frac{\langle\bar{\psi}_{+--}|H_I|\bar{\psi}'_{---}\rangle}{E_{---} - E_{+--}}|\bar{\psi}'_{+--}\rangle + \frac{\langle\bar{\psi}_{-+-}|H_I|\bar{\psi}'_{---}\rangle}{E_{---} - E_{-+-}}|\bar{\psi}'_{-+-}\rangle \\
&\quad + \frac{\langle\bar{\psi}_{--+}|H_I|\bar{\psi}'_{---}\rangle}{E_{---} - E_{--+}}|\bar{\psi}'_{--+}\rangle + \frac{\langle\bar{\psi}_{+++}|H_I|\bar{\psi}'_{---}\rangle}{E_{---} - E_{+++}}|\bar{\psi}'_{+++}\rangle + \frac{\langle\bar{\psi}_{+--}|H_I|\bar{\psi}'_{---}\rangle}{E_{---} - E_{+--}}|\bar{\psi}'_{+--}\rangle \\
&\quad + \frac{\langle\bar{\psi}_{-+-}|H_I|\bar{\psi}'_{---}\rangle}{E_{---} - E_{-+-}}|\bar{\psi}'_{-+-}\rangle \approx |\lambda'_8\rangle + \frac{\langle\bar{\psi}_{+++}|H_I|\bar{\psi}'_{---}\rangle}{E_{---} - E_{++++}}|\bar{\psi}'_{+++}\rangle.
\end{aligned} \tag{B18}$$

$$\begin{aligned}
|\Psi'_7\rangle &= |\bar{\psi}'_{+++}\rangle + \frac{\langle\bar{\psi}_{---}|H_I|\bar{\psi}'_{+++}\rangle}{E_{+++} - E_{----}}|\bar{\psi}'_{---}\rangle + \frac{\langle\bar{\psi}_{+--}|H_I|\bar{\psi}'_{+++}\rangle}{E_{+++} - E_{+--}}|\bar{\psi}'_{+--}\rangle + \frac{\langle\bar{\psi}_{-+-}|H_I|\bar{\psi}'_{+++}\rangle}{E_{+++} - E_{-+-}}|\bar{\psi}'_{-+-}\rangle \\
&\quad + \frac{\langle\bar{\psi}_{--+}|H_I|\bar{\psi}'_{+++}\rangle}{E_{+++} - E_{--+}}|\bar{\psi}'_{--+}\rangle + \frac{\langle\bar{\psi}_{+++}|H_I|\bar{\psi}'_{+++}\rangle}{E_{+++} - E_{+++}}|\bar{\psi}'_{+++}\rangle + \frac{\langle\bar{\psi}_{+--}|H_I|\bar{\psi}'_{+++}\rangle}{E_{+++} - E_{+--}}|\bar{\psi}'_{+--}\rangle \\
&\quad + \frac{\langle\bar{\psi}_{-+-}|H_I|\bar{\psi}'_{+++}\rangle}{E_{+++} - E_{-+-}}|\bar{\psi}'_{-+-}\rangle \approx |\lambda'_7\rangle + \frac{\langle\bar{\psi}_{---}|H_I|\bar{\psi}'_{+++}\rangle}{E_{+++} - E_{----}}|\bar{\psi}'_{---}\rangle, \\
|\Psi'_8\rangle &= |\bar{\psi}'_{---}\rangle + \frac{\langle\bar{\psi}_{+++}|H_I|\bar{\psi}'_{---}\rangle}{E_{---} - E_{++++}}|\bar{\psi}'_{+++}\rangle + \frac{\langle\bar{\psi}_{+--}|H_I|\bar{\psi}'_{---}\rangle}{E_{---} - E_{+--}}|\bar{\psi}'_{+--}\rangle + \frac{\langle\bar{\psi}_{-+-}|H_I|\bar{\psi}'_{---}\rangle}{E_{---} - E_{-+-}}|\bar{\psi}'_{-+-}\rangle \\
&\quad + \frac{\langle\bar{\psi}_{--+}|H_I|\bar{\psi}'_{---}\rangle}{E_{---} - E_{--+}}|\bar{\psi}'_{--+}\rangle + \frac{\langle\bar{\psi}_{+++}|H_I|\bar{\psi}'_{---}\rangle}{E_{---} - E_{+++}}|\bar{\psi}'_{+++}\rangle + \frac{\langle\bar{\psi}_{+--}|H_I|\bar{\psi}'_{---}\rangle}{E_{---} - E_{+--}}|\bar{\psi}'_{+--}\rangle \\
&\quad + \frac{\langle\bar{\psi}_{-+-}|H_I|\bar{\psi}'_{---}\rangle}{E_{---} - E_{-+-}}|\bar{\psi}'_{-+-}\rangle \approx |\lambda'_8\rangle + \frac{\langle\bar{\psi}_{+++}|H_I|\bar{\psi}'_{---}\rangle}{E_{---} - E_{++++}}|\bar{\psi}'_{+++}\rangle.
\end{aligned} \tag{B19}$$

Due to weak coupling, the overlap between subspaces is small, and we have made further simplification by taking advantage of this feature. At present, we use perturbation theory to give the first-order corrected eigenvalues and eigenstates of the system, these eigenvalues also normalized

$$\begin{aligned}
\langle\Psi'_3|\Psi_3\rangle &= \langle\Psi'_6|\Psi_6\rangle = \langle\Psi'_7|\Psi_7\rangle = \langle\Psi'_8|\Psi_8\rangle = 1 + \mathcal{O}(J^2), \\
\langle\Psi'_1|\Psi_1\rangle &= \langle\Psi'_2|\Psi_2\rangle = \langle\Psi'_4|\Psi_4\rangle = \langle\Psi'_5|\Psi_5\rangle = 1.
\end{aligned} \tag{B20}$$

and it is easy to verify that these base vectors are orthogonal to each other, they can form a complete set basis.

3. Analytic solutions of the residual tangle

Assuming that the initial state of the system is $|\psi_0\rangle = |ggg\rangle$, the evolution state of the system can be written as

$$\begin{aligned}
|\psi(t)\rangle &= U(t)|\psi_0\rangle \\
&= U(t)(|\Psi_1\rangle\langle\Psi'_1| + |\Psi_2\rangle\langle\Psi'_2| + |\Psi_3\rangle\langle\Psi'_3| + |\Psi_4\rangle\langle\Psi'_4| + |\Psi_5\rangle\langle\Psi'_5| + |\Psi_6\rangle\langle\Psi'_6| + |\Psi_7\rangle\langle\Psi'_7| + |\Psi_8\rangle\langle\Psi'_8|)|\psi_0\rangle \\
&= \langle\Psi'_1|\psi_0\rangle U(t)|\Psi_1\rangle + \langle\Psi'_2|\psi_0\rangle U(t)|\Psi_2\rangle + \langle\Psi'_3|\psi_0\rangle U(t)|\Psi_3\rangle + \langle\Psi'_4|\psi_0\rangle U(t)|\Psi_4\rangle + \langle\Psi'_5|\psi_0\rangle U(t)|\Psi_5\rangle \\
&\quad + \langle\Psi'_6|\psi_0\rangle U(t)|\Psi_6\rangle + \langle\Psi'_7|\psi_0\rangle U(t)|\Psi_7\rangle + \langle\Psi'_8|\psi_0\rangle U(t)|\Psi_8\rangle \\
&= \langle\Psi'_1|\psi_0\rangle e^{-it\Lambda_1}|\Psi_1\rangle + \langle\Psi'_2|\psi_0\rangle e^{-it\Lambda_2}|\Psi_2\rangle + \langle\Psi'_3|\psi_0\rangle e^{-it\Lambda_3}|\Psi_3\rangle + \langle\Psi'_4|\psi_0\rangle e^{-it\Lambda_4}|\Psi_4\rangle + \langle\Psi'_5|\psi_0\rangle e^{-it\Lambda_5}|\Psi_5\rangle \\
&\quad + \langle\Psi'_6|\psi_0\rangle e^{-it\Lambda_6}|\Psi_6\rangle + \langle\Psi'_7|\psi_0\rangle e^{-it\Lambda_7}|\Psi_7\rangle + \langle\Psi'_8|\psi_0\rangle e^{-it\Lambda_8}|\Psi_8\rangle.
\end{aligned} \tag{B21}$$

After substituting in the corresponding eigenvalues and eigenstates, the final state is $|\psi_f\rangle = a|ggg\rangle + b(|gge\rangle + |geg\rangle + |egg\rangle) + c(|eeg\rangle + |ege\rangle + |gee\rangle) + d|eee\rangle$, where

$$\begin{aligned}
a &= \frac{1}{8\eta^3} [12e^{\frac{it\alpha}{2\eta^2}} \Omega^2 (-i\gamma + \eta + ie^{-it\eta}\gamma + \eta e^{-it\eta}) + e^{\frac{3it(\alpha-4J\gamma^2)}{2\eta^2}} (-i\gamma + \eta)^3 + e^{\frac{-3it(\alpha-4Jrr)}{2\eta^2}} (i\gamma + \eta)^3], \\
b &= \frac{\Omega e^{\frac{4itJ\beta}{\eta^2}}}{2\eta^3} [e^{it(\frac{-2J\beta}{\eta^2} + \frac{\eta}{2})} (-\eta^2 - 2\beta - i\gamma\eta) + e^{\frac{-it\alpha}{2\eta^2}} (\eta^2 + 2\beta - i\gamma\eta) + e^{\frac{it(4\eta^3-4pp-\alpha)}{2\eta^2}} (rr + i\gamma\eta) + \\
&\quad e^{\frac{-it(2\eta^3+4pp+\alpha)}{2\eta^2}} (-rr + i\gamma\eta)], \\
c &= -\frac{\Omega^2 e^{\frac{-3it(\alpha-4Jrr)}{2\eta^2}}}{2\eta^3} [i\gamma(-1 + e^{3it\eta} + 3e^{\frac{it(2pp+\eta^3)}{\eta^2}} - 3e^{\frac{2it(pp+\eta^3)}{\eta^2}}) + \eta(-1 - e^{3it\eta} + e^{\frac{it(2pp+\eta^3)}{\eta^2}} + e^{\frac{2it(pp+\eta^3)}{\eta^2}})], \\
d &= \frac{\Omega^3 e^{\frac{it\alpha}{2\eta^2}}}{\eta^3} [3 - 3e^{-it\eta} - e^{\frac{-it(2pp-\eta^3)}{\eta^2}} + e^{\frac{-2it(pp+\eta^3)}{\eta^2}}].
\end{aligned} \tag{B22}$$

in which $\alpha = 4J\beta + \eta^3$, $\beta = \gamma^2 - \Omega^2$, $pp = J(\eta^2 + 2\beta)$, and $rr = \gamma^2 - 2\Omega^2$. After normalizing the final state, the residual tangle can be obtained

$$\tau_3 = \left| \frac{A}{4\eta^{12}B^2} \right|, \tag{B23}$$

where

$$\begin{aligned}
A &= 8xv^3\Omega^6 e^{\frac{it(\alpha+24\beta J)}{2\eta^2}} + 8h^3y\Omega^6 e^{-\frac{9it(\alpha-4Jrr)}{2\eta^2}} - 3h^2v^2\Omega^6 e^{\frac{t(-3i\alpha+8i\beta J+12iJrr)}{\eta^2}} + 16x^2y^2\Omega^6 e^{\frac{i\alpha t}{\eta^2}} \\
&\quad - 24xyvh\Omega^6 e^{\frac{it(-\alpha+4\beta J+6Jrr)}{\eta^2}},
\end{aligned}$$

$$\begin{aligned}
B = & \frac{1}{32\eta^6} \left\{ (\gamma^2 + \eta^2)^3 + 96\gamma^2(\gamma^2 + \eta^2)\Omega^2 + 48\gamma^2(13\gamma^2 + 5\eta^2)\Omega^4 + 1024\Omega^6 - 48\Omega^2[\gamma^4 - \eta^2\Omega^2 + 16\Omega^4 - \gamma^2(\eta^2 - 13\right. \\
& \Omega^2)] \cos(t\eta) + [-\gamma^6 + 15\gamma^4\eta^2 - 15\gamma^2\eta^4 + \eta^6 - 48\gamma^2\beta\Omega^2 + 48(3\gamma^2 + \eta^2)\Omega^4 - 256\Omega^6] \cos(3t\eta) + 2[72(\eta^2 - \gamma^2) \\
& \Omega^4 \cos\left(\frac{3t\eta}{2} - \frac{2Jt\beta}{\eta^2}\right) + 6(\gamma^4 - 6\gamma^2\eta^2 + \eta^4)\Omega^2 \cos\left(\frac{5t\eta}{2} - \frac{2Jt(2\gamma^2 + \Omega^2)}{\eta^2}\right) + 6\Omega^2(5\gamma^4 + \eta^4 - 4\eta^2\Omega^2 - 10\gamma^2\eta^2 + \\
& 12\gamma^2\Omega^2) \cos\left(2t\eta + \frac{2Jt(\gamma^2 + 2\Omega^2)}{\eta^2}\right) + 6\Omega^2(\eta^4 - \gamma^4) \cos\left(\frac{t\eta}{2} + \frac{2Jt(2\gamma^2 + \Omega^2)}{\eta^2}\right) - 6\Omega^2(6\gamma^4 + 4\gamma^2\eta^2 - \eta^4 + 12\gamma^2 \\
& \Omega^2 + 4\eta^2\Omega^2) \cos\left(t\eta - \frac{2Jt(\gamma^2 + 2\Omega^2)}{\eta^2}\right) + 24\Omega^2(\gamma^4\Omega^2 - \eta^2\gamma^2 + 3\Omega^2\gamma^2 - \eta^2\Omega^2) \cos\left(2t\eta - \frac{2Jt(\gamma^2 + 2\Omega^2)}{\eta^2}\right) - 24 \\
& \Omega^2(\gamma^4 + \gamma^2\eta^2 + 3\gamma^2\Omega^2 + \eta^2\Omega^2) \cos\left(t\eta + \frac{2Jt(\gamma^2 + 2\Omega^2)}{\eta^2}\right) + 48\gamma\eta\Omega^2(\gamma^2 + 5\Omega^2) \sin(t\eta) + \gamma\eta(3\gamma^4 - 10\gamma^2\eta^2 + 3 \\
& \eta^4 + 48\gamma^2\Omega^2 - 48\Omega^4) \sin(3t\eta) + 48\gamma\eta\Omega^2(\gamma^2 + 2\Omega^2) \sin\left(\frac{2t(J\gamma^2 - \eta^3 + 2J\Omega^2)}{\eta^2}\right) + 144\gamma\eta\Omega^4 \sin\left(\frac{3t\eta}{2} - \frac{2Jt\beta}{\eta^2}\right) + \\
& 24\gamma\eta\Omega^2(-\gamma^2 + \eta^2) \sin\left(\frac{5t\eta}{2} - \frac{2Jt(\Omega^2 + 2\gamma^2)}{\eta^2}\right) + 12\gamma\eta\Omega^2(\gamma^2 + \eta^2) \sin\left(\frac{t\eta}{2} + \frac{2Jt(\Omega^2 + 2\gamma^2)}{\eta^2}\right) + 12\gamma\eta\Omega^2(\gamma^2 + \eta^2 \\
& + 12\Omega^2) \sin\left(t\eta - \frac{2Jt(\gamma^2 + 2\Omega^2)}{\eta^2}\right) + 144\gamma\eta\Omega^4 \sin\left(t\eta + \frac{2Jt(\gamma^2 + 2\Omega^2)}{\eta^2}\right) + 24\gamma\eta\Omega^2(-3\gamma^2 + \eta^2 - 4\Omega^2) \sin(2t + \\
& \left. \frac{2t(J\gamma^2 + 2J\Omega^2)}{\eta^2}) \right\}, \tag{B24}
\end{aligned}$$

$$\begin{aligned}
\text{where } x = & e^{-\frac{it(2pp-\eta^3)}{\eta^2}} - e^{-\frac{2it(\eta^3+pp)}{\eta^2}} + 3e^{-i\eta t} - 3, \quad y = \frac{1}{8}(\eta+i\gamma)^3 e^{-\frac{3it(\alpha-4Jrr)}{2\eta^2}} + \frac{1}{8}(\eta-i\gamma)^3 e^{\frac{3it(\alpha-4\gamma^2J)}{2\eta^2}} + \frac{3}{2}\Omega^2(\eta-i\gamma)e^{\frac{i\alpha t}{2\eta^2}} + \\
& \frac{3}{2}\Omega^2(\eta+i\gamma)e^{\frac{i(\alpha-2i\eta^3)}{2\eta^2}}, \quad v = -(2\beta+i\gamma\eta+\eta^2) e^{-\frac{it(4\beta J-\eta^3)}{2\eta^2}} - (rr-i\gamma\eta) e^{-\frac{it(\alpha+2\eta^3+4pp)}{2\eta^2}} + (rr+i\gamma\eta) e^{-\frac{it(\alpha-4\eta^3+4pp)}{2\eta^2}} + \\
& (2\beta-i\gamma\eta+\eta^2) e^{-\frac{i\alpha t}{2\eta^2}}, \quad h = 3i\gamma e^{\frac{2it(\eta^3+pp)}{\eta^2}} - 3i\gamma e^{\frac{it(\eta^3+2pp)}{\eta^2}} - i\gamma e^{3i\eta t} + i\gamma - \eta e^{\frac{2it(\eta^3+pp)}{\eta^2}} - \eta e^{\frac{it(\eta^3+2pp)}{\eta^2}} + \eta e^{3i\eta t} + \eta.
\end{aligned}$$

4. Concrete entanglement preparation process for the truly \mathcal{PT} -symmetric system

In the analysis of entanglement preparation, we here examine the evolution dynamics of the system. In the absence of coupling between the qubits, i.e., $J = 0$ rad/ μ s, three qubits evolve independently, the evolution dynamics of states $|ggg\rangle$ and $|eee\rangle$ exhibit Rabi-like oscillation with the period of $\tau = 2\pi/\eta \sim 1.16$ μ s (the duration required to complete a Rabi oscillation of the decoupled single qubit), wherein a π phase is accumulated over a complete Rabi cycle [Figs. 9(a) and (b)]. Considering the coupling between the qubits, i.e., $J = 0.001$ rad/ μ s [Figs. 9(c) and (d)], the evolution dynamics of states $|ggg\rangle$ and $|eee\rangle$ reveal deviations from perfect Rabi oscillation. The weak inter-qubit coupling leads to imperfect dynamic evolution, preventing a complete return to the initial state within each periodic cycle. After several cycles, the high-degree entanglement of the system is prepared with the degree of entanglement $\tau_3 = 0.999$. For the normalized maximal entangled state $|\psi'_m\rangle$, the coefficients are $a_1 = 0.5656e^{i0.9\pi}$, $a_2 = a_3 = a_5 = 0.2354e^{-i0.243\pi}$, $a_4 = a_6 = a_7 = 0.2519e^{i1.248\pi}$, and $a_8 = 0.5687e^{i1.39\pi}$, the normalization factor of the pre-normalized state approaches 1, representing an exponential increase over the loss-only system. Moreover, the preparation time for maximal entanglement is about 11.6 μ s, twice as rapid as the loss-only scenario and three orders of magnitude more efficient than the conventional Hermitian system.

5. All lossy EP system

The eigenvalues are shown in Fig. 10(a) for the passive \mathcal{PT} -symmetric system, the eigenvalue of the system always has an imaginary part, which means that the probability amplitude of the state decreases exponentially with time during the evolution of the system. From Fig. 10(b), we can see the residual tangle reaches its maximal value after several oscillations over time after selecting the optimal Ω for the preparation of triplet entanglement. For the trade-off relation, the upper bound of the residual tangle oscillates with the different success rates due to the different optimal drive amplitudes, as shown in Fig. 10(c), where the optimal parameter $\{\Omega, t\}$ for a specific τ_3 is identified from the Fig. 10(b). Here we point out that the ideal state for calculating the success rate is $|\psi_i\rangle$ is the GHZ state.

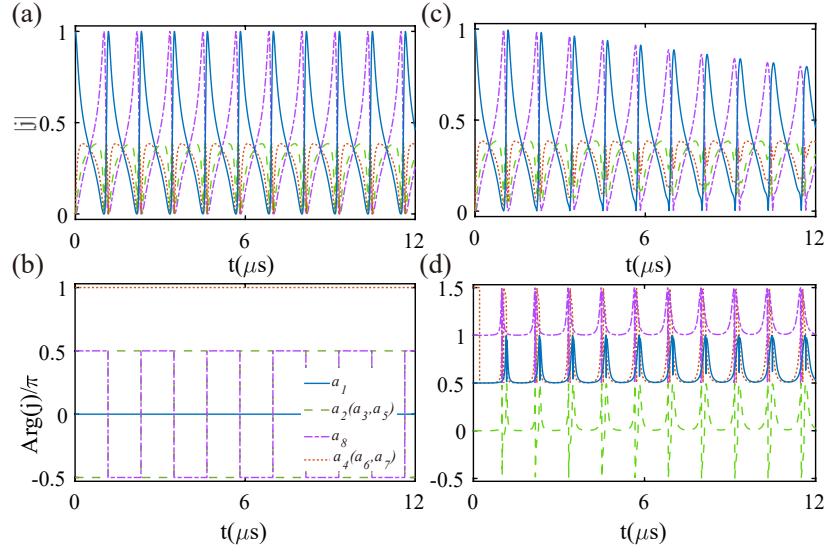


FIG. 9. Time evolution of the modulus $|a_j|$ (a) and auxiliary angle $\text{Arg}(a_j)$ (b) for each of eight complex amplitudes of the triplet state with the coupling $J = 0 \text{ rad}/\mu\text{s}$. The evolution of modulus $|a_j|$ (c) and auxiliary angle $\text{Arg}(a_j)$ (d) for the coupling $J = 0.001 \text{ rad}/\mu\text{s}$.

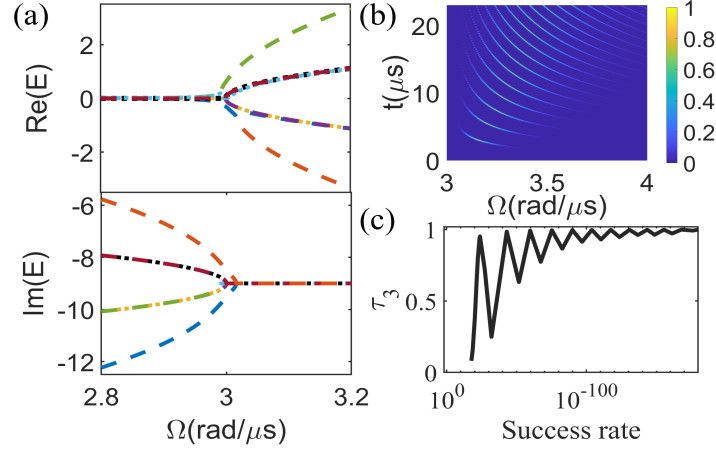


FIG. 10. (a) Real and imaginary of the eigenvalues for the passive \mathcal{PT} -symmetric system. (b) The residual tangle as the function of the drive and evolution time. (c) The maximum residual tangle that can be achieved with different success rates, where $\gamma = 12 \mu\text{s}^{-1}$ and $J = 0.001 \text{ rad}/\mu\text{s}$.

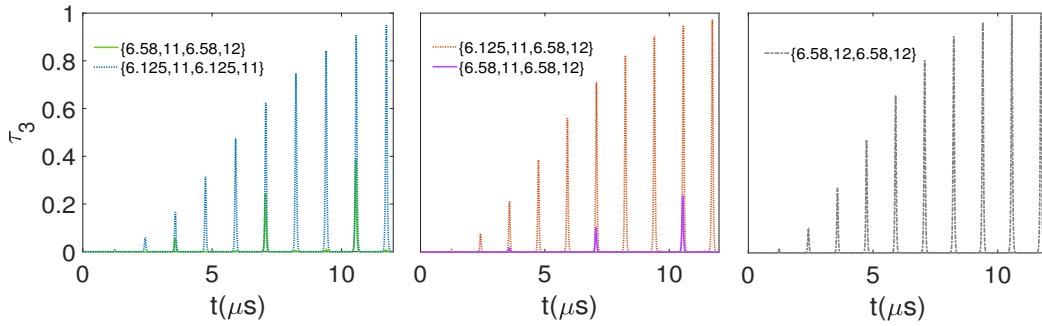


FIG. 11. The evolution of residual tangle for three qubits with different parameters $\{\Omega_2(\text{rad}/\mu\text{s}), \gamma_2(\mu\text{s}^{-1}), \Omega_3(\text{rad}/\mu\text{s}), \gamma_3(\mu\text{s}^{-1})\}$, where $\Omega_1 = 6.58 \text{ rad}/\mu\text{s}$ and $\gamma_1 = 12 \mu\text{s}^{-1}$ are fixed. The parameters of the second qubit and the third qubit are shown in the legend, where the initial state and coupling between the qubits are $|ggg\rangle$ and $J = 0.001 \text{ rad}/\mu\text{s}$, respectively.

6. Robust against the difference between qubits for the truly \mathcal{PT} -symmetric system

Furthermore, employing identical parameters for all three qubits poses experimental challenges. However, it is fortunate that as long as the same period is maintained among the three qubits, a high degree of entanglement can still be achieved in the prepared entangled state. As illustrated in Fig. 11, it is evident that when the coupling strength between the qubits is altered while maintaining the energy level, there is a significant decrease in residual tangle. Nevertheless, when condition $4\Omega_1^2 - \gamma_1^2 = 4\Omega_2^2 - \gamma_2^2 = 4\Omega_3^2 - \gamma_3^2$ is satisfied, a high degree of entanglement is still preserved.

REFERENCES

- [1] R. Horodecki, P. Horodecki, M. Horodecki, and K. Horodecki, Quantum entanglement, *Rev. Mod. Phys.* **81**, 865 (2009).
- [2] A. Steane, Quantum computing, *Reports on Progress in Physics* **61**, 117 (1998).
- [3] R. Jozsa and N. Linden, On the role of entanglement in quantum-computational speed-up, *Proceedings of the Royal Society of London. Series A: Mathematical, Physical and Engineering Sciences* **459**, 2011 (2003).
- [4] P. Walther, K. J. Resch, T. Rudolph, E. Schenck, H. Weinfurter, V. Vedral, M. Aspelmeyer, and A. Zeilinger, Experimental one-way quantum computing, *Nature* **434**, 169 (2005).
- [5] J. L. O'Brien, Optical quantum computing, *Science* **318**, 1567 (2007).
- [6] D. Bouwmeester, J.-W. Pan, K. Mattle, M. Eibl, H. Weinfurter, and A. Zeilinger, Experimental quantum teleportation, *Nature* **390**, 575 (1997).
- [7] R. Ursin, F. Tiefenbacher, T. Schmitt-Manderbach, H. Weier, T. Scheidl, M. Lindenthal, B. Blauensteiner, T. Jennewein, J. Perdigues, P. Trojek, B. Ömer, M. Fürst, M. Meyenburg, J. Rarity, Z. Sodnik, C. Barbieri, H. Weinfurter, and A. Zeilinger, Entanglement-based quantum communication over 144 km, *Nature Physics* **3**, 481 (2007).
- [8] S. Olmschenk, D. N. Matsukevich, P. Maunz, D. Hayes, L.-M. Duan, and C. Monroe, Quantum teleportation between distant matter qubits, *Science* **323**, 486 (2009).
- [9] J. Yin, J.-G. Ren, H. Lu, Y. Cao, H.-L. Yong, Y.-P. Wu, C. Liu, S.-K. Liao, F. Zhou, Y. Jiang, X.-D. Cai, P. Xu, G.-S. Pan, J.-J. Jia, Y.-M. Huang, H. Yin, J.-Y. Wang, Y.-A. Chen, C.-Z. Peng, and J.-W. Pan, Quantum teleportation and entanglement distribution over 100-kilometre free-space channels, *Nature* **488**, 185 (2012).
- [10] X.-S. Ma, T. Herbst, T. Scheidl, D. Wang, S. Kropatschek, W. Naylor, B. Wittmann, A. Mech, J. Kofler, E. Anisimova, V. Makarov, T. Jennewein, R. Ursin, and A. Zeilinger, Quantum teleportation over 143 kilometres using active feed-forward, *Nature* **489**, 269 (2012).
- [11] C. F. Roos, M. Chwalla, K. Kim, M. Riebe, and R. Blatt, 'designer atoms' for quantum metrology, *Nature* **443**, 316 (2006).
- [12] M. F. Riedel, P. Böhi, Y. Li, T. W. Hänsch, A. Sinatra, and P. Treutlein, Atom-chip-based generation of entanglement for quantum metrology, *Nature* **464**, 1170 (2010).
- [13] M. Napolitano, M. Koschorreck, B. Dubost, N. Behbood, R. J. Sewell, and M. W. Mitchell, Interaction-based quantum metrology showing scaling beyond the heisenberg limit, *Nature* **471**, 486 (2011).
- [14] L. Pezzè, A. Smerzi, M. K. Oberthaler, R. Schmied, and P. Treutlein, Quantum metrology with nonclassical states of atomic ensembles, *Rev. Mod. Phys.* **90**, 035005 (2018).
- [15] C. W. Gardiner and P. Zoller, Quantum noise: A handbook of markovian and non-markovian quantum stochastic methods with applications to quantum optics (Springer, Berlin, 2004).
- [16] M. Schlosshauer, Quantum decoherence, *Physics Reports* **831**, 1 (2019).
- [17] W. H. Zurek and J. P. Paz, Decoherence, chaos, and the second law, *Phys. Rev. Lett.* **72**, 2508 (1994).
- [18] W. H. Zurek, Decoherence, einselection, and the quantum origins of the classical, *Rev. Mod. Phys.* **75**, 715 (2003).
- [19] C. M. Bender, D. C. Brody, H. F. Jones, and B. K. Meister, Faster than hermitian quantum mechanics, *Phys. Rev. Lett.* **98**, 040403 (2007).
- [20] U. Günther and B. F. Samsonov, Naimark-dilated \mathcal{PT} -symmetric brachistochrone, *Phys. Rev. Lett.* **101**, 230404 (2008).
- [21] Z.-Z. Li, W. Chen, M. Abbasi, K. W. Murch, and K. B. Whaley, Speeding up entanglement generation by proximity to higher-order exceptional points, *Phys. Rev. Lett.* **131**, 100202 (2023).
- [22] C. M. Bender and S. Boettcher, Real spectra in non-hermitian hamiltonians having \mathcal{PT} symmetry, *Phys. Rev. Lett.* **80**, 5243 (1998).
- [23] C. M. Bender, S. Boettcher, and P. N. Meisinger, \mathcal{PT} -symmetric quantum mechanics, *Journal of Mathematical Physics* **40**, 2201 (1999).
- [24] C. M. Bender, Making sense of non-hermitian hamiltonians, *Reports on Progress in Physics* **70**, 947 (2007).
- [25] R. El-Ganainy, K. G. Makris, M. Khajavikhan, Z. H. Musslimani, S. Rotter, and D. N. Christodoulides, Non-hermitian physics and pt symmetry, *Nature Physics* **14**, 11 (2018).
- [26] A. Mostafazadeh, Exact pt-symmetry is equivalent to hermiticity, *Journal of Physics A: Mathematical and General* **36**, 7081 (2003).
- [27] A. Mostafazadeh, Pseudo-Hermiticity versus PT symmetry: The necessary condition for the reality of the spectrum of a non-Hermitian Hamiltonian, *Journal of Mathematical Physics* **43**, 205 (2002).

- [28] Z. G. Yuto Ashida and M. Ueda, Non-hermitian physics, *Advances in Physics* **69**, 249 (2020).
- [29] K. G. Makris, R. El-Ganainy, D. N. Christodoulides, and Z. H. Musslimani, Beam dynamics in \mathcal{PT} symmetric optical lattices, *Phys. Rev. Lett.* **100**, 103904 (2008).
- [30] Y. Ashida, S. Furukawa, and M. Ueda, Parity-time-symmetric quantum critical phenomena, *Nature Communications* **8**, 15791 (2017).
- [31] S. Weimann, M. Kremer, Y. Plotnik, Y. Lumer, S. Nolte, K. G. Makris, M. Segev, M. C. Rechtsman, and A. Szameit, Topologically protected bound states in photonic parity-time-symmetric crystals, *Nature Materials* **16**, 433 (2017).
- [32] L. Ge and A. D. Stone, Parity-time symmetry breaking beyond one dimension: The role of degeneracy, *Phys. Rev. X* **4**, 031011 (2014).
- [33] K. Kawabata, Y. Ashida, and M. Ueda, Information retrieval and criticality in parity-time-symmetric systems, *Phys. Rev. Lett.* **119**, 190401 (2017).
- [34] L. Ge and R. El-Ganainy, Nonlinear modal interactions in parity-time (pt) symmetric lasers, *Scientific Reports* **6**, 24889 (2016).
- [35] L. Ge, Y. D. Chong, and A. D. Stone, Conservation relations and anisotropic transmission resonances in one-dimensional \mathcal{PT} -symmetric photonic heterostructures, *Phys. Rev. A* **85**, 023802 (2012).
- [36] R. Fleury, D. Sounas, and A. Alù, An invisible acoustic sensor based on parity-time symmetry, *Nature Communications* **6**, 5905 (2015).
- [37] H. Hodaei, A. U. Hassan, S. Wittek, H. Garcia-Gracia, R. El-Ganainy, D. N. Christodoulides, and M. Khajavikhan, Enhanced sensitivity at higher-order exceptional points, *Nature* **548**, 187 (2017).
- [38] Z.-P. Liu, J. Zhang, i. m. c. K. Özdemir, B. Peng, H. Jing, X.-Y. Lü, C.-W. Li, L. Yang, F. Nori, and Y.-x. Liu, Metrology with \mathcal{PT} -symmetric cavities: Enhanced sensitivity near the \mathcal{PT} -phase transition, *Phys. Rev. Lett.* **117**, 110802 (2016).
- [39] W. Chen, Ş. Kaya Özdemir, G. Zhao, J. Wiersig, and L. Yang, Exceptional points enhance sensing in an optical microcavity, *Nature* **548**, 192 (2017).
- [40] S. Yu, Y. Meng, J.-S. Tang, X.-Y. Xu, Y.-T. Wang, P. Yin, Z.-J. Ke, W. Liu, Z.-P. Li, Y.-Z. Yang, G. Chen, Y.-J. Han, C.-F. Li, and G.-C. Guo, Experimental investigation of quantum \mathcal{PT} -enhanced sensor, *Phys. Rev. Lett.* **125**, 240506 (2020).
- [41] B. Peng, Ş. K. Özdemir, F. Lei, F. Monifi, M. Gianfreda, G. L. Long, S. Fan, F. Nori, C. M. Bender, and L. Yang, Parity-time-symmetric whispering-gallery microcavities, *Nature Physics* **10**, 394 (2014).
- [42] L. Chang, X. Jiang, S. Hua, C. Yang, J. Wen, L. Jiang, G. Li, G. Wang, and M. Xiao, Parity-time symmetry and variable optical isolation in active-passive-coupled microresonators, *Nature Photonics* **8**, 524 (2014).
- [43] H. Jing, Ş. K. Özdemir, Z. Geng, J. Zhang, X.-Y. Lü, B. Peng, L. Yang, and F. Nori, Optomechanically-induced transparency in parity-time-symmetric microresonators, *Scientific Reports* **5**, 9663 (2015).
- [44] H. Hodaei, M.-A. Miri, M. Heinrich, D. N. Christodoulides, and M. Khajavikhan, Parity-time-symmetric microring lasers, *Science* **346**, 975 (2014).
- [45] W. Liu, M. Li, R. S. Guzzon, E. J. Norberg, J. S. Parker, M. Lu, L. A. Coldren, and J. Yao, An integrated parity-time symmetric wavelength-tunable single-mode microring laser, *Nature Communications* **8**, 15389 (2017).
- [46] H. Jing, S. K. Özdemir, X.-Y. Lü, J. Zhang, L. Yang, and F. Nori, \mathcal{PT} -symmetric phonon laser, *Phys. Rev. Lett.* **113**, 053604 (2014).
- [47] J. Zhang, B. Peng, Ş. K. Özdemir, K. Pichler, D. O. Krimer, G. Zhao, F. Nori, Y.-x. Liu, S. Rotter, and L. Yang, A phonon laser operating at an exceptional point, *Nature Photonics* **12**, 479 (2018).
- [48] L. Feng, Z. J. Wong, R.-M. Ma, Y. Wang, and X. Zhang, Single-mode laser by parity-time symmetry breaking, *Science* **346**, 972 (2014).
- [49] L. Feng, M. Ayache, J. Huang, Y.-L. Xu, M.-H. Lu, Y.-F. Chen, Y. Fainman, and A. Scherer, Nonreciprocal light propagation in a silicon photonic circuit, *Science* **333**, 729 (2011).
- [50] L. Yu, H. Xue, R. Guo, E. A. Chan, Y. Y. Terh, C. Soci, B. Zhang, and Y. D. Chong, Dirac mass induced by optical gain and loss, *Nature* [10.1038/s41586-024-07664-x](https://doi.org/10.1038/s41586-024-07664-x) (2024).
- [51] R. Fleury, D. L. Sounas, and A. Alù, Negative refraction and planar focusing based on parity-time symmetric metasurfaces, *Phys. Rev. Lett.* **113**, 023903 (2014).
- [52] M. Wimmer, A. Regensburger, M.-A. Miri, C. Bersch, D. N. Christodoulides, and U. Peschel, Observation of optical solitons in pt-symmetric lattices, *Nature Communications* **6**, 7782 (2015).
- [53] J. Zhang and J. Yao, Parity-time-symmetric optoelectronic oscillator, *Science Advances* **4**, eaar6782 (2018).
- [54] S. Assaworarith, X. Yu, and S. Fan, Robust wireless power transfer using a nonlinear parity-time-symmetric circuit, *Nature* **546**, 387 (2017).
- [55] M. Liertz, L. Ge, A. Cerjan, A. D. Stone, H. E. Türeci, and S. Rotter, Pump-induced exceptional points in lasers, *Phys. Rev. Lett.* **108**, 173901 (2012).
- [56] V. V. Konotop, J. Yang, and D. A. Zezyulin, Nonlinear waves in \mathcal{PT} -symmetric systems, *Rev. Mod. Phys.* **88**, 035002 (2016).
- [57] T. Gao, E. Estrecho, K. Y. Bliokh, T. C. H. Liew, M. D. Fraser, S. Brodbeck, M. Kamp, C. Schneider, S. Höfling, Y. Yamamoto, F. Nori, Y. S. Kivshar, A. G. Truscott, R. G. Dall, and E. A. Ostrovskaya, Observation of non-hermitian degeneracies in a chaotic exciton-polariton billiard, *Nature* **526**, 554 (2015).
- [58] A. K. Jahromi, A. U. Hassan, D. N. Christodoulides, and A. F. Abouraddy, Statistical parity-time-symmetric lasing in an optical fibre network, *Nature Communications* **8**, 1359 (2017).
- [59] W. Cao, C. Wang, W. Chen, S. Hu, H. Wang, L. Yang, and X. Zhang, Fully integrated parity-time-symmetric electronics, *Nature Nanotechnology* **17**, 262 (2022).
- [60] J. Zhang, L. Li, G. Wang, X. Feng, B.-O. Guan, and J. Yao, Parity-time symmetry in wavelength space within a single spatial resonator, *Nature Communications* **11**, 3217 (2020).
- [61] S. Dogra, A. A. Melnikov, and G. S. Paraoanu, Quantum simulation of parity-time symmetry breaking with a superconducting quantum processor, *Communications Physics* **4**, 26 (2021).
- [62] R. El-Ganainy, K. G. Makris, D. N. Christodoulides, and Z. H. Musslimani, Theory of coupled optical pt-symmetric structures, *Opt. Lett.* **32**, 2632 (2007).
- [63] C. E. Rüter, K. G. Makris, R. El-Ganainy, D. N. Christodoulides, M. Segev, and D. Kip, Observation of parity-time symmetry in optics, *Nature Physics* **6**, 192 (2010).

- [64] Y. Liu, T. Hao, W. Li, J. Capmany, N. Zhu, and M. Li, Observation of parity-time symmetry in microwave photonics, *Light: Science & Applications* **7**, 38 (2018).
- [65] Ş. K. Özdemir, S. Rotter, F. Nori, and L. Yang, Parity-time symmetry and exceptional points in photonics, *Nature Materials* **18**, 783 (2019).
- [66] L. Feng, R. El-Ganainy, and L. Ge, Non-hermitian photonics based on parity-time symmetry, *Nature Photonics* **11**, 752 (2017).
- [67] L. Xiao, T. Deng, K. Wang, Z. Wang, W. Yi, and P. Xue, Observation of non-bloch parity-time symmetry and exceptional points, *Phys. Rev. Lett.* **126**, 230402 (2021).
- [68] M.-A. Miri and A. Alù, Exceptional points in optics and photonics, *Science* **363**, eaar7709 (2019).
- [69] H. Zhao and L. Feng, Parity-time symmetric photonics, *National Science Review* **5**, 183 (2018).
- [70] L. Li, Y. Cao, Y. Zhi, J. Zhang, Y. Zou, X. Feng, B.-O. Guan, and J. Yao, Polarimetric parity-time symmetry in a photonic system, *Light: Science & Applications* **9**, 169 (2020).
- [71] M. Kremer, T. Biesenthal, L. J. Maczewsky, M. Heinrich, R. Thomale, and A. Szameit, Demonstration of a two-dimensional \mathcal{PT} -symmetric crystal, *Nature Communications* **10**, 435 (2019).
- [72] Y. Wu, W. Liu, J. Geng, X. Song, X. Ye, C.-K. Duan, X. Rong, and J. Du, Observation of parity-time symmetry breaking in a single-spin system, *Science* **364**, 878 (2019).
- [73] X. Zhu, H. Ramezani, C. Shi, J. Zhu, and X. Zhang, \mathcal{PT} -symmetric acoustics, *Phys. Rev. X* **4**, 031042 (2014).
- [74] C. Shi, M. Dubois, Y. Chen, L. Cheng, H. Ramezani, Y. Wang, and X. Zhang, Accessing the exceptional points of parity-time symmetric acoustics, *Nature Communications* **7**, 11110 (2016).
- [75] A. Regensburger, C. Bersch, M.-A. Miri, G. Onishchukov, D. N. Christodoulides, and U. Peschel, Parity-time synthetic photonic lattices, *Nature* **488**, 167 (2012).
- [76] Z. Zhang, Y. Zhang, J. Sheng, L. Yang, M.-A. Miri, D. N. Christodoulides, B. He, Y. Zhang, and M. Xiao, Observation of parity-time symmetry in optically induced atomic lattices, *Phys. Rev. Lett.* **117**, 123601 (2016).
- [77] K. G. Makris, R. El-Ganainy, D. N. Christodoulides, and Z. H. Musslimani, \mathcal{PT} -symmetric optical lattices, *Phys. Rev. A* **81**, 063807 (2010).
- [78] D. Yu and F. Vollmer, Spontaneous pt-symmetry breaking in lasing dynamics, *Communications Physics* **4**, 77 (2021).
- [79] M. Walter, B. Doran, D. Gross, and M. Christandl, Entanglement polytopes: Multiparticle entanglement from single-particle information, *Science* **340**, 1205 (2013).
- [80] W. K. Wootters, Entanglement of formation and concurrence, *Quantum Inf. Comput.* **1**, 27 (2001).
- [81] R. El-Ganainy, K. G. Makris, M. Khajavikhan, Z. H. Musslimani, S. Rotter, and D. N. Christodoulides, Non-hermitian physics and pt symmetry, *Nature Physics* **14**, 11 (2018).
- [82] V. Coffman, J. Kundu, and W. K. Wootters, Distributed entanglement, *Phys. Rev. A* **61**, 052306 (2000).
- [83] R. Lohmayer, A. Osterloh, J. Siewert, and A. Uhlmann, Entangled three-qubit states without concurrence and three-tangle, *Phys. Rev. Lett.* **97**, 260502 (2006).